

Islands of Chiral Solitons in Integer Spin Kitaev Chains

Erik S. Sørensen,^{1,*} Jonathon Riddell,^{1,†} and Hae-Young Kee^{2,3,‡}

¹*Department of Physics & Astronomy, McMaster University, Hamilton ON L8S 4M1, Canada.*

²*Department of Physics, University of Toronto, Ontario M5S 1A7, Canada*

³*Canadian Institute for Advanced Research, CIFAR Program in Quantum Materials, Toronto, ON M5G 1M1, Canada*

(Dated: February 6, 2023)

An intriguing chiral soliton phase has recently been identified in the $S=\frac{1}{2}$ Kitaev spin chain. Here we show that for $S=1,2,3,4,5$ an analogous phase can be identified, but contrary to the $S=\frac{1}{2}$ case the chiral soliton phases appear as islands within the sea of the polarized phase. In fact, a small field applied in a general direction will adiabatically connect the integer spin Kitaev chain to the polarized phase. Only at sizable intermediate fields along symmetry directions does the soliton phase appear centered around the special point $h_x^*=h_y^*=S$ where two *exact* product ground-states can be identified. The large S limit can be understood from a semi-classical analysis, and variational calculations provide a detailed picture of the $S=1$ soliton phase. Under open boundary conditions, the chain has a single soliton in the ground-state which can be excited, leading to a proliferation of in-gap states. In contrast, even length periodic chains exhibit a gap above a twice degenerate ground-state. The presence of solitons leaves a distinct imprint on the low temperature specific heat.

I. INTRODUCTION

Shortly after a microscopic mechanism to realize the exactly solvable $S=\frac{1}{2}$ Kitaev model defined on the two-dimensional honeycomb lattice[1] was proposed[2], intense research in generalizations of Kitaev's original model started, including other interactions, higher-spin models, and/or external magnetic field. From a materials perspective, Kitaev materials, broadly defined as materials with dominant bond-dependent interactions, possess surprisingly rich and intricate phase diagrams [3–9]. Notably, in the presence of an applied field, Kitaev models lead to a phase diagram not only depending on field strength but also on field direction, with a resulting proliferation of competing phases. Of particular interest are field-induced spin liquid phases, where intriguing results been suggested in recent experiments on the $S=\frac{1}{2}$ material α -RuCl₃ when an in-plane field [10–14] or out-of-plane field [15] is applied. In theoretical studies of $S=\frac{1}{2}$ antiferromagnetic (AFM) Kitaev honeycomb models, signatures of possible spin liquid phases under a magnetic field have also been reported. [16–23] Near the ferromagnetic (FM) Kitaev regime, a field-induced intermediate phase was found when the magnetic field is at or close to the out-of-plane direction [24–27].

Another focus has been higher spin Kitaev models with $S > \frac{1}{2}$ [28, 29]. Initially an academic problem, a microscopic theory showed that utilizing Hund's coupling in transition metal cations and spin-orbit coupling at anions led to a higher-spin Kitaev interaction [30]. In particular, $S=1$ models [31–35] where the presence of a gapless spin liquid phase for AFM Kitaev model at finite field has been suggested [36]. While these field-induced magnetically disordered phases in $S=\frac{1}{2}$ and higher- S are fascinating, the precise nature of these phases and the physical mechanisms giving rise to them is still

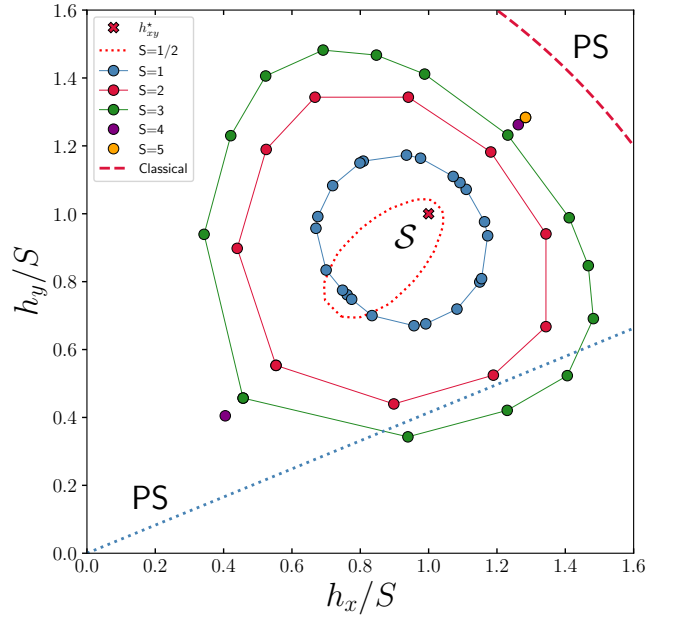


FIG. 1. iDMRG results for the $S=1$ (blue), 2 (red), 3 (green), 4 (purple), 5 (orange) Kitaev spin chain. Points indicate peaks in χ_h^e or $\chi_{\phi_{xy}}^e$. The dashed red line indicate the classical value for the transition to the polarized state, and the dotted red line are results for $S=\frac{1}{2}$ from Ref. [37]. The red cross indicates $h_{x,y}^*=S\sqrt{2}$ with $h_x^*/S = h_y^*/S = 1$.

not completely understood. One challenge is associated with the size of the systems that one can access in numerical studies.

To gain insight into the field-induced phases, a different route was recently taken, instead starting with low-dimensional versions of the Kitaev model such as chains and ladders under a magnetic field where highly precise results can be obtained for very large systems or in the thermodynamic limit. While geometrically restricted, interesting chiral phases near AFM Kitaev region in a perpendicular field have

* sorenson@mcmaster.ca

† Jonathon.Riddell@utoronto.ca

‡ hykee@physics.utoronto.ca

been identified [38] in $S=\frac{1}{2}$ ladder models. An extended soliton phase induced by the field in the $S=\frac{1}{2}$ Kitaev spin chain was also recently discovered [37].

An early work by Sen et al. [39] showed that the spin- S Kitaev chains have an analog of the Z_2 conserved quantities present in Kitaev's honeycomb model and demonstrated that there is a qualitative difference between the integer and half-integer spin due to their different commutation relations. They also showed that the $S=1$ chain exhibits a unique ground state with local excitations of the Z_2 conserved quantities, which was later confirmed by numerical studies [40]. It is then natural to ask if the field-induced soliton phase arise in Kitaev spin chains with integer spins, a question we answer in the affirmative here.

The rest of the paper is organized as follows. We present the model Hamiltonian and a main result of the phase diagram in field strength and direction in the next section. In section III we briefly summarize the main numerical techniques we have used. Section IV presents our iDMRG and DMRG results used for determining the phase diagram, excitation gaps, chiral ordering as well as the soliton mass and size. Section V describes the uniform product states approximating the two ground-states within the soliton phase for any S with periodic boundary conditions. A variational picture based on previous results for the $S=\frac{1}{2}$ model in Ref. [37] is then developed in In section VI, and penultimately we discuss in section VII how signatures of the solitons can be detected in the specific heat, in particular for open boundary conditions. Finally, in section VIII we present a discussion of our results and remaining open problems.

II. MODEL, PHASE DIAGRAM AND PHENOMENOLOGY

The Kitaev spin chain is described by the Hamiltonian:

$$\mathcal{H} = K \sum_j (S_{2j+1}^x S_{2j+2}^x + S_{2j+2}^y S_{2j+3}^y) - \sum_j \mathbf{h} \cdot \mathbf{S}_j, \quad (1)$$

where we set $g=\hbar=\mu_B=1$ and consider the AFM model with $K=1$. Furthermore, we parameterize the field term as $\mathbf{h}=\mathbf{h}(\cos \phi_{xy} \cos \theta_z, \sin \phi_{xy} \cos \theta_z, \sin \theta_z)$ and define $|\mathbf{h}|$ as the field strength. We use N to denote the number of sites in the model, and we shall refer to the $KS^x S^x$ coupling as a x -bond (--) and the $KS^y S^y$ coupling as a y -bond (--). The $S > \frac{1}{2}$ Kitaev chain was considered in Ref. [39] and the $S=1$ model in zero field has been the subject of several studies [40–43], however, to our knowledge the phase diagram in the presence of a magnetic field has not previously been investigated, likely since it has been assumed that the model would transition to the polarized phase without any intervening non-trivial phases as has been shown to be the case for the $S=\frac{1}{2}$ chain in a transverse magnetic field [44]. However, it turns out that if more general field directions are considered a highly non-trivial soliton phase can be identified in the $S=\frac{1}{2}$ chain [37], appearing along the field directions $\phi_{xy}=\frac{\pi}{4}+n\frac{\pi}{2}$.

As we show in section II A and IV A, for integer S , the soliton phase appears as an unusual *reentrant* island arising

out of the sea of the polarized state (PS). If the magnetic field already has forced the chain to enter the polarized phase, the appearance of a non-trivial soliton phase as the magnetic field is further increased may at first sight seem counterintuitive. However, at the unique field strength h_{xy}^* we identify two *exact* ground-states for any S with periodic boundary conditions (PBC), which allows us to develop variational arguments showing that such a soliton phase indeed must exist in the vicinity of h_{xy}^* . Furthermore, the existence of such a soliton phase appears to rely on the presence of a gap for periodic boundary conditions, while open boundary conditions should give rise to numerous in-gap states. We mainly focus on the integer spin case since the low field physics of the half integer spin chains is subtly different [37] but we expect many of our results, in particular the existence of the soliton phase, to be valid for any S .

Our main results for the phase diagram of the integer spin Kitaev chain, Eq. (1), are summarized in Fig. 1 where the soliton phase is shown in the first h_x, h_y quadrant for $S=1, 2, 3, 4$ and 5. By symmetry, a similar phase diagram applies to the other 3 quadrants in the h_x, h_y plane with $\phi_{xy}=\frac{\pi}{4}+n\frac{\pi}{2}$. As discussed in section V, in the classical limit we expect solitons to be present for any $h_{xy}/K < 2S$ along the line $h_x = h_y$ and the fact that the size of the soliton phase is growing with S is consistent with this. On the other hand, it is clear that the soliton phase shrinks as S is decreased. Surprisingly, as was shown in [37], it survives in the $S=\frac{1}{2}$ limit as indicated in Fig. 1 by the dotted red line.

Solitons in spin chains have been studied from the late seventies starting with the work of Mikeska [45, 46] and Fogedby [47, 48] and several reviews and monographs are now available [49–52]. At the same time, solitons in conducting polymers have been investigated [53]. Initially, classical ferromagnetic (FM) models with an easy-axis Ising symmetry were considered, where two equivalent ground-states can be identified. It is then straightforward to see that domain walls can be formed between the ground-states which should be regarded as topological solitons linking distinguishable ground-states [52] as opposed to hydrodynamic or non-topological solitons that cannot exist at rest [52]. In the continuum approximation, the sine-Gordon model is then applicable, leading to the well known kink solutions describing the domain walls. Experiments on the 1D easy-plane ferromagnetic chain system CsNiF₃ [54] confirmed the presence of solitons and subsequent studies of 1D anti-ferromagnetic materials TMMC [55, 56], CsCoBr₃ [57, 58] and CsMnBr₃ [59–61] also validated the existence of solitons excitations. Domain walls between degenerate ground-states in dimerized spin chains, such as the $S=\frac{1}{2}$, J_1 - J_2 model, have also been viewed as solitons [62–67] and observed experimentally in BiCu₂PO₆ above a critical field [68] as well as in CuGeO₃ [69]. However, in all cases one associates a *positive* mass, $\Delta_s > 0$, with the soliton which appear as an *excitation* above the ground-state and never as the unique ground-state as we find here. One might argue against this on the grounds that for N odd a single soliton is always present in the dimerized chains, however, the energy is still higher than the comparable even N system indicating a positive mass of the soliton.

Before turning to a detailed presentation of our results in section IV, V, VI and VII it is useful to give a largely phenomenological overview of the central mechanism and physics behind the soliton phase which we do in the following.

A. Phenomenological Description of the Soliton Phase

At the phenomenological level, we may understand the appearance of the soliton phase along the $h_x=h_y$ field direction in the following way. At high fields, all the spins align with the field, and we are in the polarized state (PS). Since the spins on all the bonds are aligned in a parallel manner, there is a large energy cost arising from the Ising Kitaev terms on each bond that has to be overcome to sustain the polarized state. As the field is lowered the Zeeman term is not enough to overcome this energy cost, instead the chain enters one of the following two product states

$$|XY\rangle = |xyxy\dots\rangle, \quad |YX\rangle = |yxxy\dots\rangle. \quad (2)$$

Here $|x\rangle$ and $|y\rangle$ refer to eigen-states of S^x and S^y and $|XY\rangle$ is shorthand for the state with $|x\rangle$ on odd sites and $|y\rangle$ on even sites. These two degenerate states are selected because the contribution to the energy from the Kitaev terms is identically zero. On the other hand, the spins are still partially aligned with the field so the Zeeman term lowers the energy. Crucially, as we discuss further in section V, the $|XY\rangle$ and $|YX\rangle$ are *exact ground-states* for the chain at a field $h_x^*=h_y^*=KS$ and consequently $h_{xy}^* = SK\sqrt{2}$ for *any* S under periodic boundary conditions (PBC) with energy $-NKS^2$ as long as N is even as dictated by the two site unit cell. This follows from the fact that at h_{xy}^* the Hamiltonian, Eq.(1), can be written in the following form:

$$\begin{aligned} \mathcal{H} &= \mathcal{H}_p - NKS^2 \\ \mathcal{H}_p &= K \sum_j [(S - S_{2j+1}^x)(S - S_{2j+2}^x) + \\ &\quad (S - S_{2j+2}^y)(S - S_{2j+3}^y)]. \end{aligned} \quad (3)$$

From the form of Eq. (3), it is clear that $|XY\rangle$ and $|YX\rangle$ are the only eigen-states of \mathcal{H}_p with an eigenvalue of zero. Furthermore, \mathcal{H}_p is positive semidefinite proving that $|XY\rangle$ and $|YX\rangle$ are ground-states. The field value h_{xy}^* is indicated as a green dotted line in Figs. 2, 6,7, 9. At other field strengths $h_{xy} \neq h_{xy}^*$, within the soliton phase, the two-fold degeneracy of the ground-state remain exact even for finite N but the degenerate states are now distorted from the simple $|XY\rangle$ and $|YX\rangle$ forms.

1. Open Boundary Conditions, Soliton Mass, Δ_b

Let us now consider the case of open boundary conditions (OBC) where the first bond is a x -bond ($-$). We want to see if there are other simple product states with even lower energy

than the $|XY\rangle$ and $|YX\rangle$ states that can be considered with OBC. To that end, we consider states of the form

$$|\psi_b(i)\rangle = |YX\dots \nearrow_i \dots XY\rangle, \quad (4)$$

transitioning from $|y\rangle$ on odd and $|x\rangle$ on even sites to the opposite pattern at site i where the spin is aligned with the field, thereby maximizing the Zeeman term at that site. We then need to consider what happens to the Kitaev terms neighboring the \nearrow defect. There are two possibilities:

$$|\psi_b(i)\rangle = |y-x-\boxed{y-\nearrow_i-x}-y-x-y-x-y\rangle, \quad (5)$$

and

$$|\psi_b(i)\rangle = |y-x-y-\boxed{x-\nearrow_i-y}-x-y-x-y\rangle, \quad (6)$$

we immediately see that due to the highly bond dependent interaction and the fact that the chain starts with an x -bond ($-$), the energy cost of the two bonds neighboring the defect continue to be zero, since the \nearrow_i-x occurs on an y -bond with S^y acting on $|x\rangle$ yielding zero and the $y-\nearrow_i$ on a x -bond with S^x acting on $|y\rangle$. The ψ_b state therefore lowers the energy with respect to the $|YX\rangle$ state without incurring an energy penalty. We emphasize that this effect applies equally well to odd and even N . A state such as ψ_b , transitioning between two ground-states, is a typical example of a topological soliton linking distinguishable ground-states [51, 52, 70]. One may consider other forms than the states Eq. (5) and Eq. (6) for the transition between the two ground-states, and in Ref. [37] we considered conceptually simpler bond defects which are convenient for $S=1/2$. However, since all such states are non-orthogonal, this only leads to minor differences in the final results.

Having successfully found a low-energy product state with a single defect, it is natural to consider two defects. However, if the defects are on neighboring sites, $\nearrow_i \nearrow_{i+1}$, it is clear that a large energy cost is associated with the $[i, i+1]$ bond since the spins are aligned across an antiferromagnetic bond. A second defect therefore needs to be separate from the first, creating a transition back to the YX pattern. In order to gain intuition about such a transition, let us consider 'anti-defect' states of the form

$$|B\rangle = |XY\dots \nearrow_i \dots YX\rangle, \quad (7)$$

transitioning from $|x\rangle$ on odd and $|y\rangle$ on even sites to the opposite pattern at site i where the spin is aligned with the field. As before, such a state lowers the energy by aligning the spin with the field at site i . However, something rather extraordinary happens when we consider the bond dependent Kitaev terms neighboring this anti-defect. They can take one of the two generic forms

$$|\psi_B(i)\rangle = |x-y-\boxed{x-\nearrow_i-y}-x-y-x-y-x\rangle, \quad (8)$$

and

$$|\psi_B(i)\rangle = |x-y-x-\boxed{y-\nearrow_i-x}-y-x-y-x\rangle, \quad (9)$$

in this case transitioning from the XY to the YX pattern at bond i . However, in this case the anti-defect incurs a high energy penalty from the Kitaev terms since the $y_- \nearrow_i$ now occurs on a y -bond and the $\nearrow_i - x'$ on a x -bond. Remarkably, we see that if the chain starts with a x -bond, there is no way to introduce an anti-defect from $|YX\rangle$ to $|XY\rangle$ without incurring a large energy penalty. On the other hand, a single defect from $|YX\rangle$ to $|XY\rangle$ clearly lowers the energy. It follows that in the ground-state with OBC a single soliton is present and the presence of several spatially separated solitons is energetically prohibited. However, as we discuss in section VI excited states of a single soliton exists leading to a proliferation of low-lying excitations.

We note that, starting the chain with a y -bond ($-$) with a defect, transitioning from the $|XY\rangle$ to the $|YX\rangle$ pattern merely interchanges the roles of ψ_b and ψ_B . Furthermore, the ψ_b and ψ_B states are not eigen-states of the Hamiltonian but, considering all possible states of the form, $|\psi_b(i)\rangle$ leads to a good description of the low-energy subspace for OBC. In section VI we discuss variational calculations within such a subspace, and for clarity we reserve the name 'soliton' for linear combinations of the states $\Psi_b = \sum a_i |\psi_b(i)\rangle$. For OBC, within such a variational subspace, we can then determine by how much the presence of the soliton lowers the energy with respect to the $|YX\rangle$ state, which we define as the soliton mass, Δ_b . From the above, we expect that within the soliton phase,

$$\Delta_b < 0, \quad (10)$$

otherwise the ground-state would not be a single soliton state. On the other hand, the $|\psi_B(i)\rangle$ are high energy states that in isolation presumably are of little relevance. However, it is still very useful to consider linear combinations $\Psi_B = \sum c_i |\psi_B(i)\rangle$ thereby estimating the energy cost of an anti-soliton. In an analogous manner we can then define the anti-soliton mass Δ_B and, within the soliton phase, we expect $\Delta_B > 0$, reflecting the energy cost associated with the anti-soliton. Even though a state such as Ψ_B is not expected to be close to an eigen-state, Δ_B should still be a good estimate of the energy cost of an anti-soliton and soliton anti-soliton bB states could be of low-energy and therefore relevant for periodic boundary conditions which we discuss next.

2. Periodic Boundary Conditions - Spin Gap

If we now consider periodic boundary conditions (PBC) it is clear that excitations out of the $|XY\rangle, |YX\rangle$ states must involve both a defect and anti-defect which we refer to as bB states. Another remarkable feature of the soliton phase in the Kitaev chain is that there is no symmetry relation between the defect and anti-defect. In other systems where related physics can be observed such as the dimerized phase of the $S=\frac{1}{2}, J_1-J_2$ model, where $S=\frac{1}{2}$ domain walls between degenerate ground-states have been viewed as solitons [62–67], the soliton and anti-soliton are effectively indistinguishable and both raise the energy and both carry a spin of $S=\frac{1}{2}$. Here, the opposite is true, the defect and anti-defect are clearly distinguishable with the defect lowering the energy while the anti-

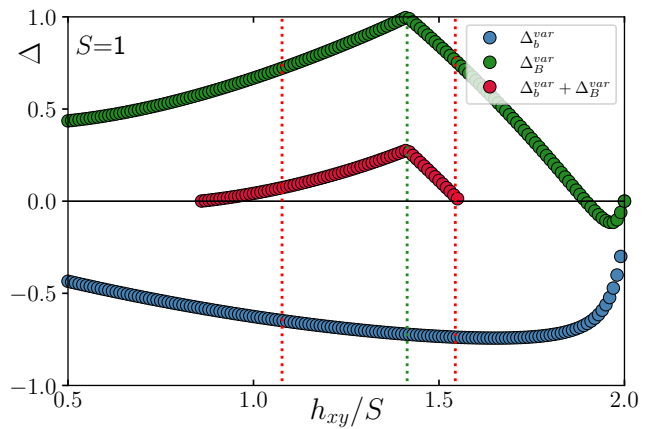


FIG. 2. Variational estimates with OBC, $N=100$ and $S=1$ of the soliton mass, Δ_b , and anti-soliton mass Δ_B as a function of field h_{xy} shown with the resulting estimate of the spin gap, $\Delta_b + \Delta_B$. Only for a finite range of fields is the spin gap positive and the soliton phase stable. The dotted red lines are the critical fields h_{xy}^{c1} and h_{xy}^{c2} obtained from iDMRG, the green dotted line is h_{xy}^* .

defect raises the energy ($\Delta_b < 0, \Delta_B > 0$). The defect and anti-defect are also not eigen-states of the spin operators and a definite spin cannot be associated, and we cannot ascribe the presence of the soliton to an unpaired spin. Furthermore, it turns out that the anti-defect raises the energy more than the defect lowers it. If we now imagine a defect and anti-defect well enough separated in a periodic system that their interaction can be neglected, this asymmetry in the energy cost then leads to a spin-gap above the two degenerate ground-states. Even though the anti-defect is rather costly, the combination of the defect and anti-defect has a much smaller energy cost, creating a modest spin-gap. Not surprisingly, the maximum of the spin-gap appears to coincide with h_{xy}^* where the $|XY\rangle$ and $|YX\rangle$ product states are exact ground-states. In fact, it is clear that we must have:

$$\Delta_b + \Delta_B > 0, \quad (11)$$

within the soliton phase, and we can take $\Delta_b + \Delta_B$ to be a first approximation to the spin gap for PBC. Consider the opposite to be true, in that case for OBC a state with bBb would have lower energy than b , and $bBbBb$ even lower energy, leading to a contradiction. Eq (11) may therefore be seen as providing an estimate of the extent of the soliton phase.

3. Critical Fields, h_{xy}^{c1}, h_{xy}^{c2}

As we shall discuss further in section VI, for fields $h_{xy} \neq h_{xy}^*$ the states $|XY\rangle$ and $|YX\rangle$ that form degenerate ground-states at h_{xy}^* cease to be exact ground-states, although the ground-state in the soliton phase is always two-fold degenerate. Instead, an approximation to the ground-states can be found by considering the closely related product states of the form

$$|X'Y'\rangle = |x'y'x'y' \dots\rangle, \quad |Y'X'\rangle = |y'x'y'x' \dots\rangle. \quad (12)$$

where the states $|x'\rangle$ and $|y'\rangle$ are not orthogonal but instead at an angle *exceeding* 90 degrees by a small amount δ in either direction, justifying the $|x'\rangle$, $|y'\rangle$ notation. For such states the spins are partly aligned with the field and the Zeeman term can still lower the energy considerably, however, as long as $h_{xy} < h_{xy}^*$ an additional lowering of the energy can be obtained from the Kitaev term if $\delta > 0$. If we consider a small $\delta > 0$ then to linear order, each Kitaev term then lowers the energy by $-KS^2\delta$ while the average Zeeman term will change to $-Sh_{xy}(1-\delta)/\sqrt{2}$ increasing the energy by $+Sh_{xy}\delta/\sqrt{2}$. Hence, if $h_{xy} < h_{xy}^*$, a non-zero $\delta > 0$ can lower the energy justifying the notation $|x'\rangle$ and $|y'\rangle$. For $h_{xy} > h_{xy}^*$, δ changes sign and the angle between $|x'\rangle$, $|y'\rangle$ is smaller than 90 degrees quickly approaching the PS state which is reached when $\delta = -\pi/4$. We note that, for small δ , the states $|X'Y'\rangle$ and $|Y'X'\rangle$ are still degenerate and linearly independent but no-longer orthogonal.

The presence of a non-zero δ implies that the soliton mass, Δ_b and anti-soliton mass, Δ_B vary with h_{xy} , as does the energy of the states $|Y'X'\rangle$ and $|X'Y'\rangle$ with respect to which they are defined. As we discuss further in section VI it is possible to perform variational calculations to determine the optimal Ψ_b and Ψ_B as a function of h_{xy} thereby obtaining variational estimates for the masses Δ_b^{var} and Δ_B^{var} versus h_{xy} . Such estimates should be relatively precise, close to h_{xy}^* progressively failing as the field is tuned away from h_{xy}^* . If we use Eq. (11) to define the soliton phase we can then use $\Delta_b^{var} + \Delta_B^{var} > 0$ to estimate the extent of the soliton phase. Our variational results (see section VI) for Δ_b^{var} and Δ_B^{var} are shown in Fig. 2 for $S=1$ as a function of h_{xy} along with their sum. Crucially, there is only a finite range around h_{xy}^* where $\Delta_b^{var} + \Delta_B^{var} > 0$ and the soliton phase is stable, indicating a lower, h_{xy}^{c1} , and upper h_{xy}^{c2} critical field. The critical fields can also be determined very precisely from iDMRG calculations, which are indicated as the dotted red lines in Fig. 2. The variational estimate for h_{xy}^{c2} is in surprisingly good agreement with the iDMRG result, while the variational estimate of h_{xy}^{c1} is significantly worse. As we discuss in section IV, the agreement of the variational estimates with precise DMRG results for Δ_b progressively worsens as the field is tuned away from h_{xy}^* . Nevertheless, the fact that the simple variational calculations predict the existence of a non-zero lower critical field, h_{xy}^{c1} , is highly non-trivial and consistent with the fact that the soliton phase appears as an island in the polarized sea (the PS state).

B. The Kitaev Chain at $\mathbf{h}=0$

The Kitaev chain in zero field has a number of invariants similar to the plaquette operators defined for the Honeycomb model [1]. As shown in Ref. 39, if site operators

$$\mathcal{R}_l^x = e^{i\pi S_l^x}, \quad \mathcal{R}_l^y = e^{i\pi S_l^y} \quad (13)$$

are defined, then, with x -bond (y -bond) couplings in \mathcal{H} , Eq. (1), between $[l, l+1]$ with l odd(even), bond-parity op-

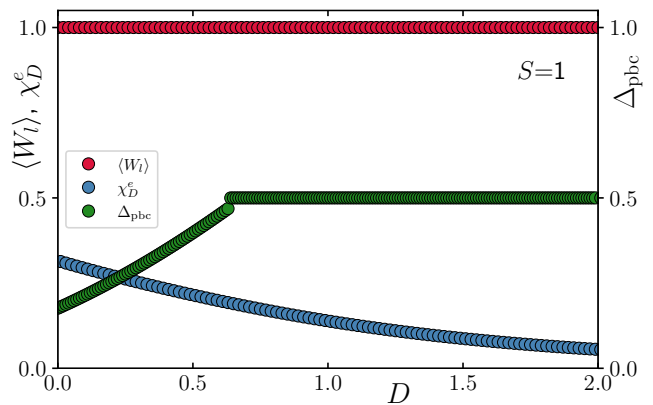


FIG. 3. iDMRG results for the bond-parity operator $\langle W_l \rangle$ and susceptibility χ_D^e as a function of D for the $S=1$ Hamiltonian \mathcal{H}_D , Eq. (18). Results are shown alongside finite DMRG results with PBC for the spin gap, Δ_{pbc} for $N=60$. A smooth evolution with h_{xy} is evident and no transition is observed.

erators W_l can be defined on odd and even bonds[42]

$$W_{2l-1} = \mathcal{R}_{2l-1}^y \mathcal{R}_{2l}^y, \quad W_{2l} = \mathcal{R}_{2l}^x \mathcal{R}_{2l+1}^x, \quad (14)$$

that commutes with the Hamiltonian, $[W_l, \mathcal{H}] = 0$, and for integer S , amongst themselves $[W_l, W_k] = 0$. The W_l are therefore invariants and it can be shown that the ground-state lies in the sector with all $\langle W_l \rangle = 1$ and for PBC it is non-degenerate. For half-integer S , W_l anti-commutes with, $W_{l\pm 1}$ making the physics of the half-integer spin Kitaev chain distinct from the case of integer S that we consider here.

In materials other interactions than the Kitaev interactions will be present and the $S=1$ Kitaev chain has been studied in the presence of an additional Heisenberg coupling, J [42, 43], a Γ -term [40] and also in the presence of anisotropy [41, 71]. However, it is important to consider in detail the nature of the zero field ground-state of the isotropic $S=1$ chain with $J=\Gamma=0$. In Ref. [42, 43] the ground-state at $\mathbf{h}=0$ was described as a quantum spin liquid, however, in Ref. [40] it was noted that the entanglement spectrum is not doubled and concluded it is not a symmetry protected topological (SPT) state [72–74]. Following Ref. 75 we have therefore investigated the projective representations, U that can be obtained from the mixed transfer matrices in iDMRG. In general, if the site symmetries, \mathcal{R}^x and \mathcal{R}^y are respected their representations can differ by a phase that must be ± 1 :

$$U(\mathcal{R}^x)U(\mathcal{R}^y) = \pm U(\mathcal{R}^y)U(\mathcal{R}^x). \quad (15)$$

It is then convenient to isolate the phase factor by defining [75]:

$$\mathcal{O}_{Z_2 \times Z_2} \equiv \frac{1}{\chi} \text{Tr} (U(\mathcal{R}^x)U(\mathcal{R}^y)U^\dagger(\mathcal{R}^x)U^\dagger(\mathcal{R}^y)), \quad (16)$$

with χ the bond dimension. For the $S=1$ Kitaev chain at $\mathbf{h}=0$ we find $\mathcal{O}_{Z_2 \times Z_2} = 1$. Similarly, under time reversal one finds that at $\mathbf{h}=0$

$$\mathcal{O}_{\text{TR}} \equiv \frac{1}{\chi} \text{Tr} (U_{\text{TR}} U_{\text{TR}}^*) = 1, \quad (17)$$

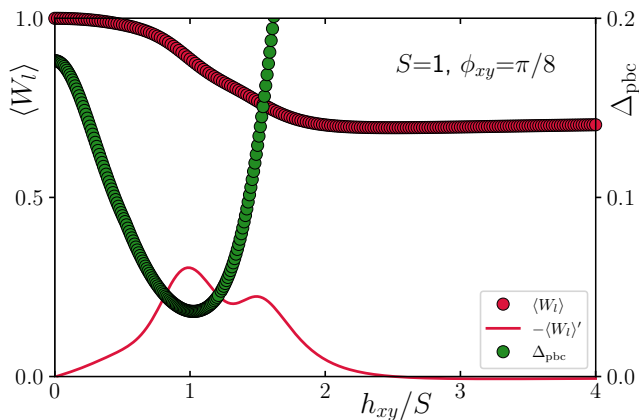


FIG. 4. iDMRG results with $S=1$ for the bond-parity operator $\langle W_l \rangle$ and its derivative $\langle W_l \rangle'$ as a function of h_{xy}/S at an angle $\phi_{xy} = \pi/8$ in the h_x, h_y plane shown alongside finite DMRG results with PBC for the spin gap, Δ_{pbc} for $N=60$. A smooth evolution with h_{xy} is evident and no transition is observed.

with \star denoting complex conjugation and χ the bond dimension. Finally, if inversion is considered, one again finds that the trivial phase factor $\mathcal{O}_T=1$. This is in contrast to the Haldane phase of the $S=1$ spin chain where it is known that $\mathcal{O}_{Z_2 \times Z_2}=-1$, $\mathcal{O}_{\text{TR}}=-1$ in addition to a non-trivial phase factor of $\mathcal{O}_T=-1$ when considering inversion [76, 77]. For $S=1$ we can illustrate the trivial nature of the ground-state of the Kitaev chain at $\mathbf{h}=0$ by adding an easy-plane crystal field term, D of the form $D \sum_j (S_j^z)^2$ to the $\mathbf{h}=0$ Hamiltonian to obtain

$$\mathcal{H}_D = K \sum_j (S_{2j+1}^x S_{2j+2}^x + S_{2j+2}^y S_{2j+3}^y) + D \sum_j (S_j^z)^2. \quad (18)$$

Note that, the D -term preserves the symmetries present at $\mathbf{h}=0$ in Eq. (1). In the $D \rightarrow \infty$ limit, the ground-state of Eq. (18) is the trivial product-state $|0\rangle|0\rangle|0\rangle \dots$. We can now study the evolution of \mathcal{H}_D as D is increased from zero. In Fig. 3 we show iDMRG results for $\langle W_l \rangle$ which remain a constant $\langle W_l \rangle=1$ for any D . The gap Δ_{pbc} increases with D and never approaches zero, likewise, the energy susceptibility χ_D^e quickly goes monotonically to zero. The evolution is smooth, and no transition is observed, consistent with the trivial nature of the ground-state at $\mathbf{h}=0$. Without breaking the symmetry, we have connected the two states. This defines what is sometimes called a symmetry protected trivial phase [78, 79] (SPT) or alternatively a trivial SPT phase [80].

It is known that any SPT phase can be connected to the same trivial product state if we break the symmetry [72, 73, 81, 82]. In our determination of the phase diagram in section IV A this turns out to be an important point since, as already shown in Fig. 1, the soliton phases appear as isolated islands within the polarized state implying that a path can be found between the $\mathbf{h}=0$ and $h_{xy}=\infty$ ground-states without an intervening phase transition. We note that, in contrast to the D term discussed above, the introduction of a field term at a general angle will break most symmetries present in the Hamil-

tonian, Eq. (1). For $S=1$ we can demonstrate the absence of a transition by calculating $\langle W_l \rangle$ and Δ_{pbc} as a function of h_{xy} which should interpolate smoothly between $\mathbf{h}=0$ and the large field limit where the simple product state associated with complete field polarization is the ground-state. iDMRG results for such a calculation are shown in Fig. 4 where $\langle W_l \rangle$ is graphed versus h_{xy}/S along with finite DMRG results for the spin gap, Δ_{pbc} for $N=60$. The calculations are done at a fixed angle $\phi_{xy}=\pi/8$ shown as the dotted blue line in Fig. 1, that does not intersect with the soliton phase for $S=1$. As is clear from the results in Fig 4 the evolution is smooth, and no transition is observed, although some structure in $\langle W_l \rangle'$ can be observed in the proximity of the soliton phase where Δ_{pbc} also has a minimum. In summary, for $S=1$ we therefore conclude that the $\mathbf{h}=0$ phase is a symmetry protected trivial (SPT) phase. Once the field is applied in a general direction, the symmetry is broken, and there is no distinction between the SPT and polarized states. However, along the unique directions $h_x = \pm h_y$ a transition to the soliton phase is possible since the chain is still protected by the combined symmetry operation of a rotation on each site by π around the field direction, $\mathcal{R}^{xy}=\exp(i\pi(S^x + S^y)/\sqrt{2})$, followed by a translation by one lattice spacing, T . We expect this to hold for all integer S but the half-integer case is distinct, as discussed in [37] for $S=\frac{1}{2}$, since the $\mathcal{R}^{xy} \otimes T$ symmetry protection allow for a critical line to be present along the $h_x = \pm h_y$ symmetry directions, connecting the soliton phase to $\mathbf{h}=0$.

III. NUMERICAL METHODS

In the following we present results mainly obtained from finite size density matrix renormalization group [83–88] (DMRG) using both periodic (PBC) and open (OBC) boundary conditions as well as from infinite DMRG [88, 89] (iDMRG) techniques. For the iDMRG calculations, we use a unit cell of either 12 or 24 sites. We note that well converged iDMRG results should yield results in the thermodynamic limit free of finite-size effects independent of the size of the unit cell. Typical precisions for both DMRG and iDMRG are $\epsilon < 10^{-11}$ with a bond dimension in excess of 1000. In order to establish the phase diagram, we focus on the following susceptibilities. With e_0 the ground-state energy per spin, we define the energy susceptibilities

$$\chi_h^e = -\frac{\partial^2 e_0}{\partial h^2}, \quad \chi_{\phi_{xy}}^e = -\frac{\partial^2 e_0}{\partial \phi_{xy}^2}, \quad \chi_{\theta_z}^e = -\frac{\partial^2 e_0}{\partial \theta_z^2} \quad (19)$$

where h is the field strength and ϕ_{xy} and θ_z the field angles. Here, χ_h^e is effectively a magnetic susceptibility. At a quantum critical point (QCP) it is known [90] that, for a finite system of size N , the energy susceptibility diverges as

$$\chi^e \sim N^{2/\nu-d-z}. \quad (20)$$

Here ν and z are the correlation and dynamical critical exponents and d is the dimension. We see that χ^e only diverges at the phase transition if the critical exponent ν is smaller than

$2/(d+z)$. In the present case $d=1$ and we assume $z=1$, so $\nu < 1$ if a divergence is observed.

In section VII we present thermodynamic results for the specific heat as a function of temperature. The results are obtained using purification [81, 91–96] where the density matrix ρ acting on a physical Hilbert space \mathcal{H}^P is represented as a pure state $|\psi\rangle$ in an enlarged space $\mathcal{H}^P \otimes \mathcal{H}^A$:

$$\rho = \text{Tr}_A |\psi\rangle\langle\psi|, \quad (21)$$

where the ancillary space \mathcal{H}^A can be taken to be identical to \mathcal{H}^P . This gives the thermofield double purification [97, 98] (TFD)

$$|\psi_\beta\rangle = \frac{1}{\sqrt{Z}} \sum_n e^{-\beta E_n/2} |n\rangle_P |n\rangle_A, \quad (22)$$

where $|n\rangle$ are the eigenvectors and E_n the eigenvalues of \mathcal{H} and thermal expectation values of an operator \mathcal{O} can be obtained from $\langle\psi_\beta|\mathcal{O}|\psi_\beta\rangle$. The TFD can be obtained by using imaginary-time evolution $|\psi_\beta\rangle \sim e^{-\beta\mathcal{H}/2}|\psi_0\rangle$ starting from a state $|\psi_0\rangle = \prod_i \frac{1}{\sqrt{d}} \sum_{\sigma_i} |\sigma_i\rangle_P |\sigma_i\rangle_A$, where σ_i runs over the local Hilbert space of dimension d . On a given site, the physical and ancillary degrees of freedom are then maximally entangled in the state $|\psi_0\rangle$. For the calculations presented in section VII imaginary time evolution with a time step of 0.001 is used.

IV. DMRG AND IDMRG RESULTS

A. Phase Diagram

Our results for the phase diagram for $S=1, S=2, S=3$, and to a lesser extent also for $S=4,5$ are summarized in Fig. 1 where the extent of the soliton phase in the h_x, h_y plane is shown as obtained from iDMRG results for χ_h^e and $\chi_{\phi_{xy}}^e$. Remarkably, the soliton phase appears as an *island* in the polarized sea since the PS state completely surrounds the soliton phase, as we have discussed above. For $S=1$ this is illustrated in Fig. 5(c) where $\chi_{\phi_{xy}}^e$ is shown for the field values $h_{xy}/K=0.8$ and 1.3 . As the field angle ϕ_{xy} is varied, clear transitions are visible for $h_{xy}/K=1.3$, but completely absent for $h_{xy}/K=0.8$. If instead the field strength, h_{xy} is varied at a field angle of $\phi_{xy}=\pi/4$ then two very well-defined transitions are clearly visible in Fig. 5(a) for both $S=1$ and $S=2$. The peak positions are what is plotted in Fig. 1. We have extensively search for a phase transition distinguishing the low-field phase ($h_{xy} < h_{xy}^{c1}$) from the PS state using different techniques and different paths through the phase diagram, but it appears adiabatically connected to the PS phase as explicitly shown in section II B. This is likely unique to the integer spin models, since for $S=1/2$ results indicate the presence of a critical line [37] for $h_{xy} < h_{xy}^{c1}$.

The soliton phase is not only restricted to the h_x, h_y plane, but extends to non-zero θ_z . This is demonstrated in Fig. 5(b) where iDMRG results for $\chi_{\theta_z}^e$ versus θ_z are shown at the fixed field values of $h_{xy}/K=1.3$ and $h_{xy}/K=2.6$ for $S=1$ and $S=2$

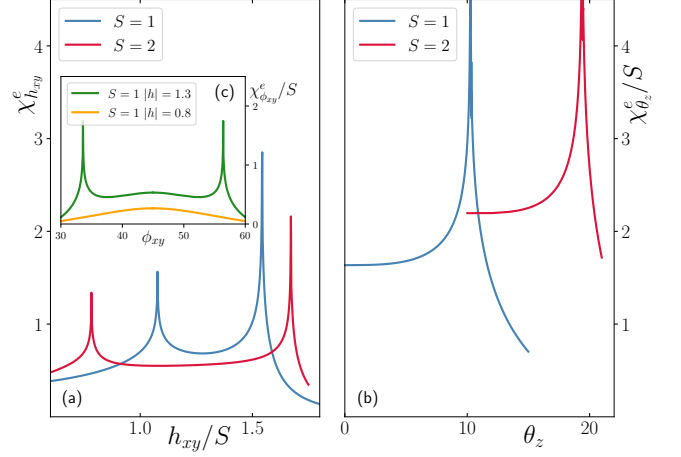


FIG. 5. (a) iDMRG results for $\chi_{h_{xy}}^e$ versus the field strength h_{xy}/S for the $S=1$ and $S=2$ Kitaev spin chains, showing the positions of the critical fields h_{xy}^{c1} and h_{xy}^{c2} . (b) iDMRG results for the $S=1$ and $S=2$ Kitaev spin chains, showing $\chi_{\theta_z}^e/S$ versus the field angle θ_z for field strengths of $|h|/K=1.3$ ($S=1$) and 2.6 ($S=2$). (c) iDMRG results for the $S=1$ Kitaev spin chain for $\chi_{\phi_{xy}}^e$ versus the field angle ϕ_{xy} for field strengths of $|h|/K=0.8$ and 1.3 . Note the absence of transitions for $|h|/K=0.8$

respectively. Clear transitions are observed at the critical angles $\theta_z=10.27^\circ$ ($S=1$) and 19.41° ($S=2$).

B. Energy Gaps

We next turn to a discussion of the energy spectrum at fixed field angles $\theta_z=0$, $\phi_{xy}=\pi/4$ as a function of field strength, h_{xy} and for brevity we only discuss the $S=1$ chain. Due to the rapid growth of the size of the Hilbert space with N it is convenient to use finite size DMRG calculations to determine the ground- (E_0) and excited- (E_n) state energies and study the gaps ($\Delta_n=E_n-E_0$) in the spectrum. Our results are shown in Fig. 6.

We first focus on PBC, where our results are shown in Fig. 6(b). We exclusively consider, N even dictated by the two-site unit cell. The ground-state at $h_{xy}=0$ is non-degenerate below a sizable gap, $\Delta_{\text{pbc}}(h_{xy}=0)=0.1763K$ in agreement with previous results [42]. The first excited state at $h_{xy}=0$ is known to be N -fold degenerate [39, 42]. At $h_{xy}^{c1}=1.077K$ the gap closes, and the soliton phase is entered. Within the soliton phase for $h_{xy}^{c1} < h_{xy} < h_{xy}^{c2}=1.544K$ the ground-state is exactly two-fold degenerate, even for finite N , below a sizable gap. As mentioned previously, the maximum of the gap coincides with the presence of the two exact product ground-states $|YX\rangle$ and $|XY\rangle$ at h_{xy}^* (indicated as the green dotted line in Fig. 6(b)) where the gap is estimated to be $\Delta_{\text{pbc}}(h_{xy}=0)=0.2555K$.

We then turn the attention to OBC (Fig. 6(a)) where the ground-state at $h=0$ is four-fold degenerate for $S=1$ [42, 71]. For small fields, the ground-state degeneracy is lifted, and a low-lying doublet appears below a singlet. At field strengths

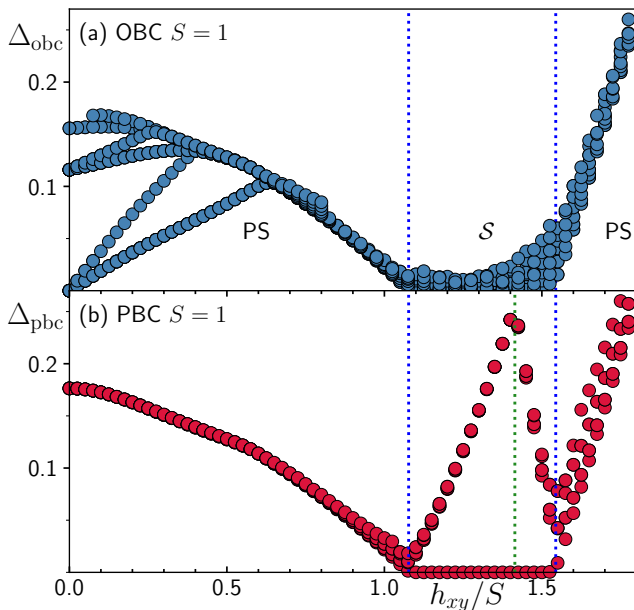


FIG. 6. DMRG results for the first few excited states as a function of field, h_{xy} at $\phi_{xy}=45^\circ$ and $\theta_z=0$ for the $S=1$ Kitaev spin chain. The critical fields delineating the soliton phase are indicated by the dotted blue lines. (a) Results for OBC with $N=100$. At $h_{xy}=0$ the ground-state is four-fold degenerate. Note the proliferation of low-lying states in the soliton phase, marked by 'S'. (b) Results for PBC with $N=60$. Note, the two-fold degenerate ground-state in the soliton phase. The green dotted line indicates $h_{xy}^*=SK\sqrt{2}$.

$h_{xy} \sim 0.4 - 0.6$ the low-lying singlet and doublet merge with the other low-lying states which we assume might form the lower edge of a continuum. When the lower critical field h_{xy}^{c1} is reached the gap closes and throughout the soliton phase, marked as S in Fig. 6, a proliferation of low-lying states is visible until the upper critical field $h_{xy}^{c2}=1.544K$ is reached where the chain transitions back into the polarized state and a gap opens up. Within the soliton phase the DMRG results for the gaps indicate significant finite-size corrections which we have not been able to analyze in detail, and it has not been possible to determine if these low-lying states correspond to a true gapless spectrum as opposed to a significant number of discrete in-gap levels appearing within the gap present for periodic boundary conditions. The ground-state degeneracy, if any, within the soliton phase for OBC is also an open question.

The difference in the spectrum within the soliton phase is rather remarkable, even more so since the spectrum for OBC does not depend on the parity of N and occurs equally well for N even and odd. As discussed in the introduction, the absence of $SU(2)$ symmetry means that it is difficult to explain the multitude of low-lying states occurring for OBC as arising from unpaired degrees of freedom.

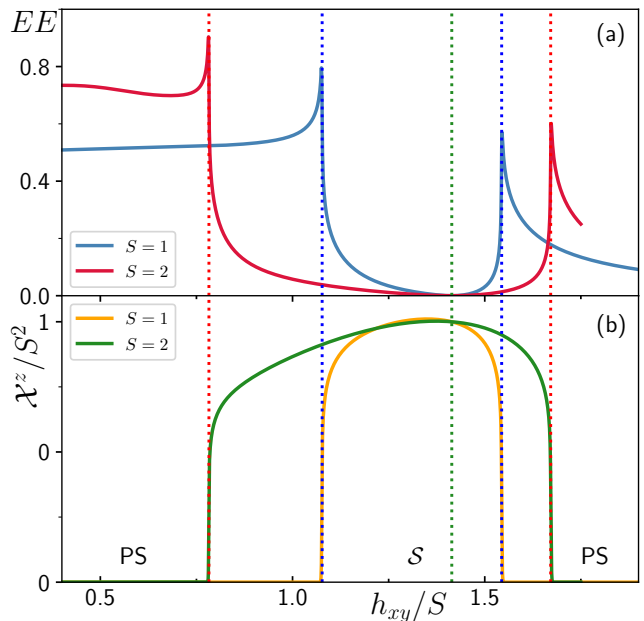


FIG. 7. iDMRG results for the $S=1$ and $S=2$ Kitaev spin chains. The dashed lines indicate the critical fields h_{xy}^{c1} and h_{xy}^{c2} . (a) The entanglement entropy EE versus the field strength h_{xy}/S . Note that very low EE in the soliton phase. (b) The z -component of the vector chirality scaled with S^2 , χ^z/S^2 , versus h_{xy}/S .

C. Chiral Order, χ^z and Entanglement

In light of the two exact ground-states $|YX\rangle$ and $|XY\rangle$ occurring at h_{xy}^* for PBC it is not surprising that the soliton phase can be characterized by a non-zero vector chirality, χ^α :

$$\chi^\alpha = (-1)^j \langle (\mathbf{S}_j \times \mathbf{S}_{j+1})^\alpha \rangle. \quad (23)$$

While $\chi^{x,y}=0$ in the soliton phase, $\chi^z \neq 0$ as was previously established for $S=\frac{1}{2}$. This is shown in Fig. 7(b) for $S=1$ and $S=2$ where iDMRG results for χ^z are plotted as a function of h_{xy}/S . As can be seen, χ^z remains sizable throughout the soliton phase reaching a maximum close to (or at) h_{xy}^* before abruptly going to zero at h_{xy}^{c1} and h_{xy}^{c2} . The soliton phase should then be regarded as a chiral soliton phase.

In Fig. 7(a) we show results for the bipartite entanglement entropy:

$$EE = -\text{Tr} \rho_A \ln \rho_A \quad (24)$$

where ρ_A is the reduced density for half the system. The states $|YX\rangle$ and $|XY\rangle$ are only *exact* ground-states for PBC and the iDMRG results shown in Fig. 7(a) are obtained for OBC. Hence at h_{xy}^* , shown as the green dotted line in Fig. 7, the entanglement entropy EE is not strictly zero, as should be the case for an exact product state, but rather extremely small. As is clearly visible in Fig. 7(a), EE peaks at h_{xy}^{c1} and h_{xy}^{c2} but away from the quantum critical points it remains rather small throughout the entire soliton phase, approaching zero at h_{xy}^* , implying that the ground-state is close to a product state within the soliton phase.

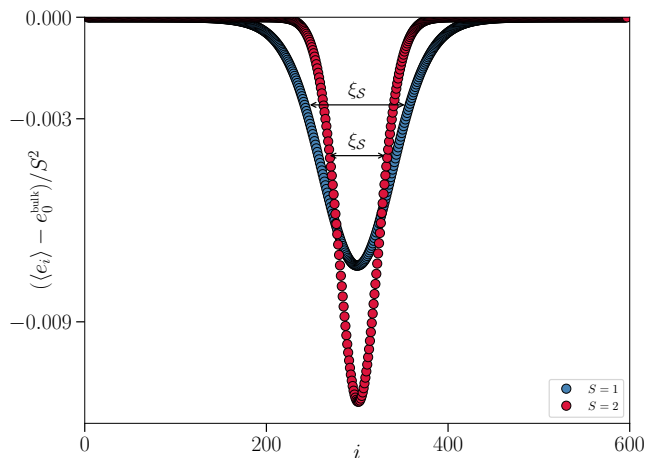


FIG. 8. Finite size DMRG results with $N=600$ for the $S=1$ (blue) and $S=2$ (red) Kitaev spin chains showing the relative energy density $\langle (e_i) - e_0^{\text{bulk}} \rangle / S^2$ versus position, i , in the chain. Results are shown for $h_{xy}/K=1.32$ ($S=1$) and $h_{xy}/K=2.60$ ($S=2$)

D. Soliton Mass, Δ_b and Width, ξ_S

The variational calculation of the soliton mass for OBC described in section II A 1 and VI relies on a subtractive procedure where the energy of the single soliton state is measured with respect to the isotropic product state. For a more detailed understanding of the DMRG results it is useful to have a more refined measure of Δ_b that does not involve a subtraction. In the absence of $SU(2)$ symmetry and a well defined spin for the soliton it is then necessary to focus on the local bond energy density which we define as the energy of the bond $[i, i+1]$ plus $1/2$ the field terms on the sites i and $i+1$. Far away from the soliton the energy density attains a constant value e_0^{bulk} and we expect that this bulk energy density is essentially identical to the energy density of the two fold degenerate ground-states with PBC. It is then instructive to study the following quantity:

$$\langle e_i \rangle - e_0^{\text{bulk}} \quad (25)$$

This is shown in Fig. 8 where $\langle e_i \rangle - e_0^{\text{bulk}}$ is plotted versus i for $h_{xy}/K=1.32$ ($S=1$) and 2.60 ($S=2$), showing a sharply localized soliton. Furthermore, the soliton 'sharpen's' with increasing S , displaying a smaller spatial extent. We can now simply define the soliton mass, Δ_b , as the integrated deviation from e_0^{bulk} in the following manner:

$$\Delta_b = \sum_i (\langle e_i \rangle - e_0^{\text{bulk}}). \quad (26)$$

Clearly, this measures by how much the soliton has lowered the total energy which was our original definition of the soliton mass, Δ_b .

From high precision DMRG calculations with OBC on $N=1200$ sites for a range of h_{xy} we can now extract Δ_b for both $S=1$ and $S=2$. Our results are illustrated in Fig. 9(a) where Δ_b/S^2 is shown as a function of h_{xy} . As one might

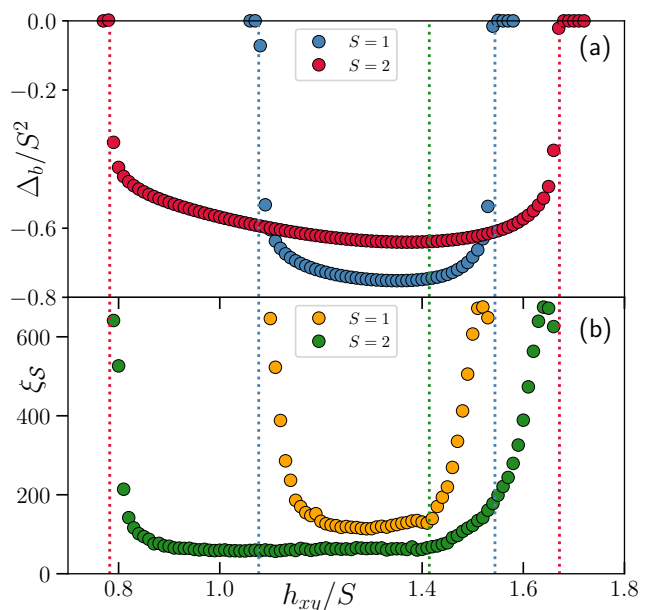


FIG. 9. Finite size DMRG results with $N=1200$ for the $S=1$ and $S=2$ Kitaev spin chains. The dashed lines indicate the critical fields h_{xy}^{c1} and h_{xy}^{c2} . (a) The soliton mass, Δ_b/S^2 versus the field strength h_{xy}/S . (b) The soliton size ξ_S versus h_{xy}/S .

expect, Δ_b is roughly proportional to S^2 , consistent with classical models of solitons [49], and with only a modest variation throughout the soliton phase. In contrast to the variational results for Δ_b^{var} shown in Fig. 2 the DMRG results in Fig. 9(a) show that Δ_b tends to zero at h_{xy}^{c1} and h_{xy}^{c2} . From the definition, Eq. (26) it follows that $\Delta_b=0$ outside the soliton phase where we expect the energy density to be uniform. In contrast, the variational states ψ_b can never yield a uniform energy density, and we have to use a less refined measure for the soliton mass. However, it is still useful to compare the estimates at h_{xy}^* , where we from DMRG for $S=1$ find $\Delta_b=-0.7457$ and from the variational calculations $\Delta_b^{\text{var}}=-0.7225$, in good agreement.

The energy profiles shown in Fig. 8 can be used to estimate the size of the soliton, ξ_S by simply measuring at what distance $|\langle e_i \rangle - e_0^{\text{bulk}}|$ has decreased by a factor of $1/e$ from the maximum. Measures of ξ_S are indicated on Fig. 8. Using this definition of ξ_S we have determined the size of the soliton throughout the soliton phase from high precision DMRG calculations with OBC on $N=1200$ sites for both $S=1$ and $S=2$. The results are shown in Fig. 9(b). Through most of the soliton phase ξ_S remains roughly constant at around 120 lattice spacings for $S=1$ and approximately 60 lattice spacings for $S=2$, before increasing dramatically close to h_{xy}^{c1} and h_{xy}^{c2} .

V. UNIFORM PRODUCT STATES

As already discussed in section II A the product states $|YX\rangle$ and $|XY\rangle$ play a crucial role in our understanding of the soliton phase. For $\theta_z=0$, $\phi_{xy}=\pi/4$ at h_{xy}^* they are ex-

act ground-states for PBC, however, as pointed out in section II A 3, when h_{xy} is tuned away from h_{xy}^* a good approximation to the ground-state can be obtained by considering product states of the form $|Y'X'\rangle$ and $|X'Y'\rangle$ where the angle between $|y'\rangle$ and $|x'\rangle$ deviates from $\pi/2$ in both directions by an amount c . We now wish to establish a reliable estimate of the optimal value for this angle, c^* , as a function of h_{xy} for any S .

A. Estimate of c^*

In the following we focus on the case of $S=1$ and $S=2$ with generalizations to $S > 2$ straight forward. With c taking the place of δ discussed in section II A 3, we define for $S=1$ the following states on a given site:

$$\begin{aligned} |x'\rangle &= (e^{i2c}, \sqrt{2}e^{ic}, 1)/2 \\ |y'\rangle &= (e^{-i2b}, \sqrt{2}e^{-ib}, 1)/2, \end{aligned} \quad (27)$$

with $b = \pi/2 + c$, while for $S=2$ we define:

$$\begin{aligned} |x'\rangle &= (e^{i4c}, 2e^{i3c}, \sqrt{6}e^{i2c}, 2e^{ic}, 1)/4 \\ |y'\rangle &= (e^{-i4b}, 2e^{-i3b}, \sqrt{6}e^{-i2b}, 2e^{-ib}, 1)/4. \end{aligned} \quad (28)$$

We can then define the product states:

$$|X'Y'\rangle = |x'y'x'y' \dots\rangle, \quad |Y'X'\rangle = |y'x'y'x' \dots\rangle, \quad (29)$$

for both $S=1$ and $S=2$. The optimal value for the excess angle, c^* , will depend on the field h_{xy} . However, if we neglect boundary effects, then, due to the simple product nature of the states, it is only necessary to consider a two site system in order to find the optimal c^* . To proceed, we focus on a x -bond and assign half a field term to each bond and write the single bond Hamiltonian as follows:

$$\mathcal{H}_{1\text{bond}} = K S_1^x S_2^x - h_{xy}(S_1^x + S_1^y + S_2^x + S_2^y) \frac{1}{2\sqrt{2}}, \quad (30)$$

with the $1/\sqrt{2}$ arising from the field angle $\phi_{xy} = \pi/4$. Evaluating $E_{1\text{bond}} = \langle Y'X' | \mathcal{H}_{2\text{site}} | Y'X' \rangle$ we find:

$$E_{1\text{bond}} = -K S^2 \cos c \sin c - \frac{S h_{xy}}{\sqrt{2}} (\cos c - \sin c) \quad (31)$$

Minimizing $E_{1\text{bond}}$ with respect to c at a given h_{xy} yields the optimal c as

$$c^* = \tan^{-1} \left[\frac{u + \sqrt{4S^2 - u^2}}{-u + \sqrt{4S^2 - u^2}} \right] = \cos^{-1} \frac{u}{2S} - \frac{\pi}{4}, \quad (32)$$

where $u = h_{xy}/K$. It follows that c^* becomes zero at $u = h_{xy}/K = S\sqrt{2}$, coinciding with h_{xy}^* as, has to be the case. Furthermore, at $h_{xy}/K = 2S$ the optimal value for c becomes $c^* = -\pi/4$ and the spins are then fully aligned with the field for any $h_{xy} > 2SK$. This signals the transition to the PS state at the classical level and is shown as the red dashed line in Fig. 1. Using the optimal value of c^* from Eq. (32) one finds for the energy:

$$E_{1\text{bond}} = -\frac{1}{4}(2S^2 + u^2), \quad u \leq 2S. \quad (33)$$

B. Estimate of the product state defect energy

It is illustrative to also consider a single defect state, at h_{xy}^* where calculations with the states $|\psi_b(i)\rangle$ can be significantly simplified. At h_{xy}^* we may estimate the defect energy of the state

$$|d\rangle = |y_- \nearrow_i - x\rangle, \quad (34)$$

and compare it to the state $|yxy\rangle$ on just 2 bonds sites since the two states will have the same energy elsewhere. That is, we consider the 2 bond Hamiltonian:

$$\begin{aligned} \mathcal{H}_{2\text{bond}} &= K S_1^x S_2^x + K S_2^y S_3^y \\ &- \frac{h_{xy}}{\sqrt{2}} \left(\frac{1}{2}(S_1^x + S_1^y) + S_2^x + S_2^y + \frac{1}{2}(S_3^x + S_3^y) \right), \end{aligned} \quad (35)$$

again counting the field terms on the first and last site by a factor of $1/2$. At h_{xy}^* , it is straight forward to evaluate $\langle yxy | \mathcal{H}_{2\text{bond}} | yxy \rangle = -2$ and $\langle d | \mathcal{H}_{2\text{bond}} | d \rangle = -1 - \sqrt{2}$. The energy of the defect state $|d\rangle$ is then $1 - \sqrt{2} \sim -0.4142$ lower in energy than the $|yxy\rangle$ state. As discussed in section IV D, at h_{xy}^* DMRG results for Δ_b yields -0.7457 , considerably lower. Moreover, if this analysis is extended to $h_{xy} \neq h_{xy}^*$, and to include the $|x_- \nearrow_i - y\rangle$ state describing the anti-defect, then the upper critical field coincides with the classical value of $2S$ and the lower critical field is absent. We therefore need to consider a full variational calculation in the space defined by all states $|\psi_b(i)\rangle$ and $|\psi_B(i)\rangle$ which we do next. A preliminary discussion of results from such variational calculations formed we presented in sections II A 2 and II A 3.

VI. VARIATIONAL APPROACH

In order to develop a variational approach valid for an extended part of the phase diagram we generalize the single defect states in Eq. (5) and (6) to be constructed from the $|y'\rangle$ and $|x'\rangle$ states.

$$\begin{aligned} |\psi_b(i)\rangle &= |y' - x' - \boxed{y' - \nearrow_i - x'} - y' - x' - y' - x' - y'\rangle, \\ |\psi_B(i)\rangle &= |y' - x' - y' - \boxed{x' - \nearrow_i - y'} - x' - y' - x' - y'\rangle, \end{aligned} \quad (36)$$

transitioning from the $Y'X'$ to the $X'Y'$ pattern at bond i . As already noted, the energy cost of the ferromagnetically aligned $x'_i - x'$ bond is relatively small since it occurs on a y -bond. Likewise for the $y'_i - y'$ bond. As shown in Fig. 7(a) the entanglement is very low in the soliton phase and we expect such product states to be of relevance. Analogously, we define ‘anti’-defects of the form

$$\begin{aligned} |\psi_B(i)\rangle &= |x' - y' - \boxed{x' - \nearrow_i - y'} - x' - y' - x' - y' - x'\rangle, \\ |\psi_b(i)\rangle &= |x' - y' - x' - \boxed{y' - \nearrow_i - x'} - y' - x' - y' - x'\rangle, \end{aligned} \quad (37)$$

in this case transitioning from the $X'Y'$ to the $Y'X'$ pattern at bond i . As discussed, in this case the defects are now rather costly since since the $y'_i - y'$ now occurs on a y -bond and the $x'_i - x'$ on a x -bond. The defect states, ψ_b and ψ_B are slight variations of the bond defects considered for the $S=\frac{1}{2}$ Kitaev chain in Ref. [37] and are slightly more optimal for $S \geq 1$. However, since all such basis states are non-orthogonal the final results depend relatively little on the specific choice of basis states.

With the states ψ_b and ψ_B defined we can form linear combinations of these single defect states and perform a variational calculation within the single defect subspace. As illustrated in Fig. 7(a), the entanglement is very low within the soliton phase and we therefore expect such linear combinations to yield very reliable results within the soliton phase. Explicitly, we define the variational states:

$$|\Psi_b\rangle = \sum_{k=1}^N a_k |\psi_b(k)\rangle, \quad |\Psi_B\rangle = \sum_{l=2}^{N-1} g_l |\psi_B(l)\rangle. \quad (38)$$

We refer to these states as soliton and anti-soliton states to distinguish them from the individual basis states $|\psi_b(i)\rangle$ and $|\psi_B(i)\rangle$ which we refer to as defect states or basis states. Correspondingly, we distinguish between soliton energies and defect energies when referring to the energy of the linear combination and individual basis state. We also note that for Ψ_B we exclude the sites $l=1, N$ since their overlap with the lower energy $|Y'X'\rangle$ and $|X'Y'\rangle$ states is an inconvenience.

The determination of the variational coefficients, a_k and g_l is a straight forward optimization problem. Since the basis states are non-orthonormal the minimum can be found by solving the generalized eigenvalue problem (see appendix A) in terms of the matrices

$$\mathcal{H}_{kl} = \langle \psi_b(k) | H | \psi_b(l) \rangle \quad \text{and} \quad \mathcal{M}_{kl} = \langle \psi_b(k) | \psi_b(l) \rangle, \quad (39)$$

which can be solved by standard methods. The solution of the generalized eigenvalue problem, Eq. (39), determines the variational optimized ground-states, Ψ_b, Ψ_B in the sub-space formed by $|\psi_b(i)\rangle$ and $|\psi_B(i)\rangle$.

Having defined the single defect states $|\psi_b(i)\rangle, |\psi_B(i)\rangle$ it is straight forward to extend the variational calculations to two-defect bB states relevant for PBC by considering:

$$|\psi_{bB}(i, j)\rangle = \left(\boxed{y'_i - x'_i} - \boxed{y'_j - x'_j} \right) |y'_i - x'_i - y'_j - x'_j\rangle, \quad (40)$$

and defining two-soliton states of the form:

$$|\Psi_{bB}\rangle = \sum_{i \neq j} a_{i,j} |\psi_{bB}(i, j)\rangle. \quad (41)$$

Similar variational two-soliton states have previously been considered for the J_1 - J_2 $S=\frac{1}{2}$ chain [62] and $S=\frac{1}{2}$ Kitaev chain [37]. It is convenient to include the $|Y'X'\rangle$ and $|X'Y'\rangle$ states in the variational sub-space for PBC and the variational gap to two-soliton states Δ_{2sol}^{var} can then be directly obtained from the the eigenvalues of Eq. (39). For PBC we expect Δ_{2sol}^{var} of the spin gap, Δ_{pbc}

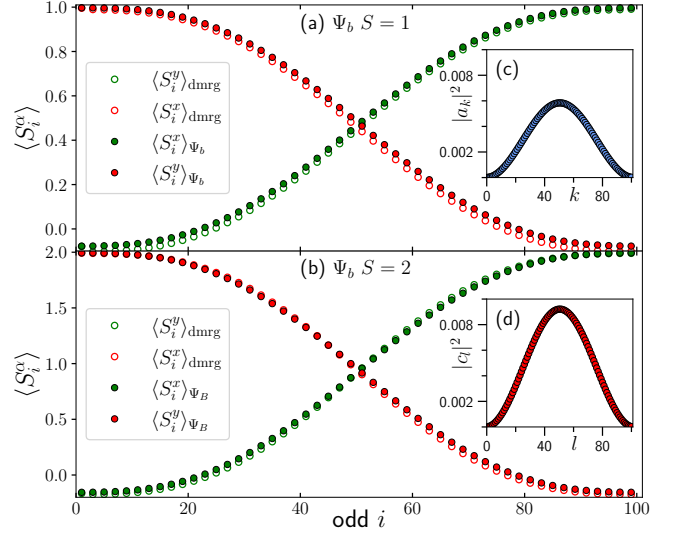


FIG. 10. $\langle S_i^\alpha \rangle$ from finite size DMRG results (open circles) with $N=100$ for the $S=1$ and $S=2$ Kitaev spin chains, compared to variational results (solid circles) for the one soliton state Ψ_b . To emphasize the presence of the soliton only odd sites are shown. (a) Results for $S=1$ at $h_{xy}/K=1.3$. (b) Results for $S=2$ at $h_{xy}/K=2.6$. (c) Variational amplitudes $|a_k|^2$ for $S=1$. (d) Variational amplitudes $|c_l|^2$ for $S=2$.

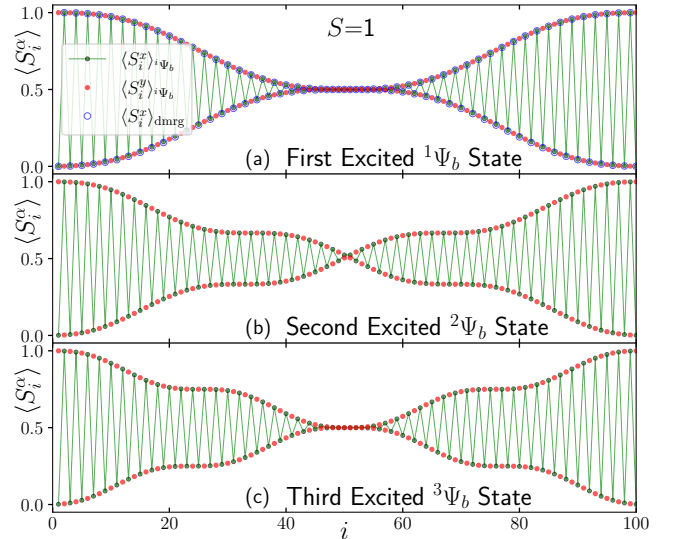


FIG. 11. $\langle S_i^\alpha \rangle$ for the $S=1$ chain at h_{xy}^* from variational calculations for the *excited* soliton state $^n\Psi_b$. (a) Results for first excited state $^1\Psi_b$, compared to finite size DMRG results (open circles) for $\langle S_i^\alpha \rangle_{\text{dmrg}}$ (b) Results for second excited state $^2\Psi_b$. (c) Results for third excited state $^3\Psi_b$.

A. Variational results for $S=1$

We first discuss our results for $S=1$. Representative numerical results for a few values of h_{xy} and N are collected in table I. The first check on the variational results is to directly compare the energy obtained with results from DMRG.

TABLE I. DMRG and variational, $E(\Psi_b)$, $E(\Psi_B)$, $E(Y'X')$ energies for the $S=1$ chain for different field values, h_{xy} and system sizes, N . The resulting variational estimates of Δ_b^{var} , Δ_B^{var} and $\Delta_B^{\text{var}} + \Delta_b^{\text{var}}$ and $\Delta_{2\text{sol}}^{\text{var}}$. These can be compared with DMRG results for $N=1200$ for Δ_b^{dmrg} and $N=60$ for $\Delta_{\text{pbc}}^{\text{dmrg}}$.

h_{xy}	N	DMRG	$E(\Psi_b)$	$E(\Psi_B)$	$E(Y'X')$	Δ_b^{dmrg}	Δ_b^{var}	Δ_B^{var}	$\Delta_B^{\text{var}} + \Delta_b^{\text{var}}$	$\Delta_{2\text{sol}}^{\text{var}}$	$\Delta_{\text{pbc}}^{\text{dmrg}}$
h_{xy}^*	100	-100.7453	-100.7221	-99.	-100.	-0.7457	-0.7221	1.	0.2779	0.2788	0.2555
	240	-240.7457	-240.7225	-239.	-240.		-0.7225	1.	0.2775		
1.3	100	-93.0400	-92.8743	-91.2751	-92.1725	-0.7487	-0.7018	0.8974	0.1956	0.2327	0.1549
	240	-222.3942	-222.0245	-220.4254	-221.3225		-0.7020	0.8971	0.1951		

For $S=1$ at h_{xy}^* we see that the presence of the defect lowers the energy considerably when compared to the $|Y'X'\rangle$ state for a final result that is within 0.023% ($N=100$) and 0.009% ($N=240$) of the DMRG results. This is a remarkable good agreement although we note that the agreement worsens for $h_{xy} \neq h_{xy}^*$. The agreement between Δ_b^{var} and Δ_b^{dmrg} is at the level of a few percent. A more detailed check on the variational ground-state Ψ_b with OBC can be obtained by evaluating $\langle S_i^\alpha \rangle$, $\alpha=x, y$ and comparing to DMRG results. Variational results at $h_{xy}/K = 1.3$ for the on-site magnetization (filled circles) are shown in Fig. 10(a) where only *odd* sites are plotted making the change from $|y'\rangle$ on odd sites, $|x'\rangle$ on even sites to $|y'\rangle$ on even sites, $|x'\rangle$ on odd sites, evident. The results in Fig. 10(a) for $h_{xy}/K = 1.3$ are in excellent agreement with the DMRG results shown as open circles, with the agreement even better at h_{xy}^* . For comparison, we show results for $S=2$ in Fig. 10(b) at $h_{xy}/K=2.6$ with equally good agreement between variational and DMRG results.

From the numerical results in table I it is also clear that $\Delta_B^{\text{var}} + \Delta_b^{\text{var}}$ is in good agreement with the result, $\Delta_{2\text{sol}}^{\text{var}}$, obtained directly from two-soliton variational calculations with Eq. (41) with $N=60$. Furthermore, at h_{xy}^* both estimates are in agreement with $\Delta_{\text{pbc}}^{\text{dmrg}}$ obtained from DMRG calculations on periodic chains. This can be viewed as a validation of the soliton anti-soliton picture and would indicate that interactions between the soliton and anti-soliton are relatively modest. However, from the discussion of the size of the soliton in section IV D we expect $\xi_S \sim 120$ lattice spacings in the $S=1$ soliton phase, implying that much larger variational calculations will be needed to study the soliton anti-soliton interaction in detail. Regrettably, the two-soliton calculations scale as N^2 making such calculations numerically untractable.

1. Excited single soliton states

As can be seen from table I, in the vicinity of h_{xy}^* the spin gap for PBC is sizable, of the order $\sim 0.25K$. It is then interesting to consider excited single soliton states [70, 99]. We denote such states by $^n\Psi_b$ and we can obtain reliable variational estimates for such excited states by considering the first few eigenstates when solving the generalized eigenvalue problem, Eq. (39). As is clear from the results in section IV B such excited single soliton states cause a proliferation of low-lying levels within the soliton phase at energies below the gap for PBC. Results for $^1\Psi_b$, $^2\Psi_b$ and $^3\Psi_b$ at h_{xy}^* are shown in

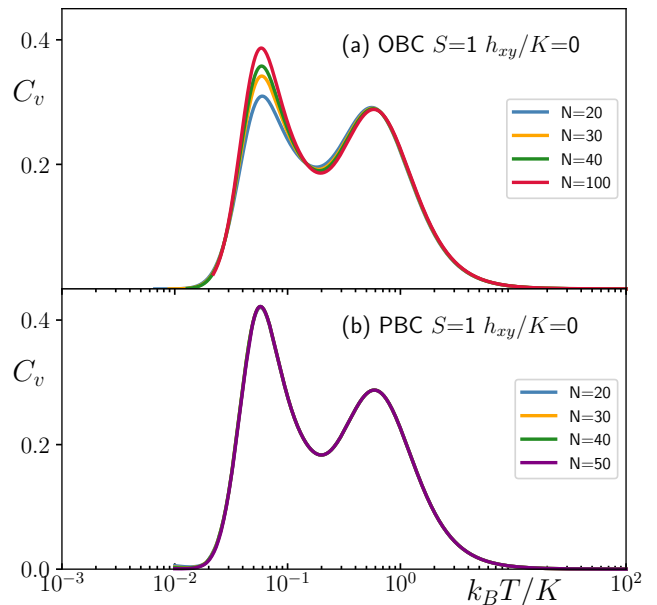


FIG. 12. The specific heat $C_v(T)$ versus $k_B T/K$ for the $S=1$ Kitaev spin chain at $h_{xy}/K=0.0$, as obtained from purification. (a) OBC, $N=20,30,40,100$. (b) PBC, $N=20,30,40,50$.

Fig. 11. For the first excited state, $^1\Psi_b$, we compare to excited state DMRG results for $\langle S_i^x \rangle$ which are in excellent agreement with the variational results. Note that in Fig. 11 results for every site is plotted while in Fig. 10 only results for *odd* sites are plotted. However, in Fig. 11 the same change from $|y'\rangle$ on odd sites, $|x'\rangle$ on even sites to $|y'\rangle$ on even sites, $|x'\rangle$ on odd sites, occurs.

VII. SPECIFIC HEAT, $S=1$

The thermodynamics of the $S=1$ Kitaev chain in zero field, $\mathbf{h}=0$, has previously been studied [40, 71] using transfer matrix renormalization group [100, 101] (TMRG) techniques and a perturbative effective Hamiltonian approach [71]. To fully account for the presence of a single soliton in the low energy spectrum for OBC which breaks translational symmetry we here use a purification method outlined in section III that does not rely on translational symmetry. We exclusively focus on the $S=1$ chain, although we expect results for other integer $S > 1$ to be relatively similar.

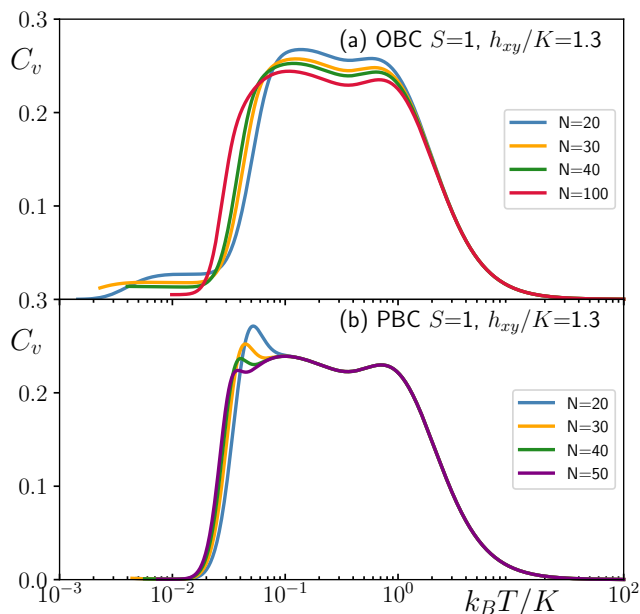


FIG. 13. The specific heat $C_v(T)$ versus $k_B T/K$ for the $S=1$ Kitaev spin chain in the middle of the soliton phase, at $h_{xy}/K=1.3$, as obtained from purification. (a) OBC, $N=20,30,40,100$. (b) PBC, $N=20,30,40,50$.

Under periodic boundary conditions at $\mathbf{h}=0$ we show our purification results in Fig. 12(b) for the $S=1$ chain for $N=20,30,40$ and 50 down to temperatures of $k_B T/K=0.01$. In complete agreement with the TMRG results from Ref. 40, finite-size effects are conspicuously absent. However, the unusual double peak structure, with peaks at $T_l/K=0.057$ and $T_h/K=0.587$ for $N=50$, of the specific heat associated with thermal fractionalization [102, 103] characteristic of Kitaev physics is clearly present arising from the separation of energy scales as previously noted [40, 71]. The low-temperature peak has been shown to arise from excitations of the bond-parity operators, W_l Eq. (14), with the average bond density, $\bar{W}_b=(1/L)\sum\langle W_l \rangle$, approaching zero at the energy scale of the low temperature peak [40, 71].

For OBC our results at $\mathbf{h}=0$ are shown in Fig. 12(a) for $N=20,30,40$ and 100. In this case there are clearly visible finite-size effects visible in the low-temperature peak. As the system size, N , is increased the low- T peak increases eventually approaching the PBC result. We note that the results presented here for $S=1$ can be straightforwardly integrated to yield the entropy. However, the results from such an integration do not show any indication of plateaus as expected to occur in the two dimensional honeycomb models [104].

The results in Fig. 12 should be contrasted with the results in Fig. 13 obtained for the $S=1$ chain close to the center of the soliton phase at $h_{xy}/K=1.3$. Compared to the $\mathbf{h}=0$ results the first observation is that the separation of energy scales present at $\mathbf{h}=0$ inducing the double peak structure is now significantly reduced and replaced with an almost constant specific heat between temperatures of $k_B T/K \sim 0.05$ although several not very well defined peaks are visible. For PBC, Fig. 13(b) it is

possible to locate 3 peaks, two of which are almost independent of N , however, the lowest temperature peak dramatically decreases with increasing system size with significant weight in C_v shifting to lower temperatures. It is natural to associate this lowest temperature peak with the bB soliton states. Within the picture we have been proposing here, where the spin gap for PBC, Δ_{pbc} in the soliton phase arises from the presence of such bB states with both a soliton and an anti-soliton, it is natural to expect rather pronounced finite-size effects due to the significant size of the solitons, $\xi_S \sim 120$ lattice spacings in the $S=1$ soliton phase. This would explain the strong size dependence of the peak. We expect a continuum of such bB states starting above the spin gap which is consistent with the results for PBC in Fig. 13(b). From the results in Fig. 6(b), we note that $\Delta_{\text{pbc}} \sim 0.1548/K$ at $h_{xy}/K=1.3$ whereas the low- T peak for $N=50$ occurs at $k_B T/K = 0.038$ implying a significant density of states starting at Δ_{pbc} .

The more interesting features of the specific heat are observed for OBC, where we show results in Fig. 13(a) at $h_{xy}/K=1.3$ for $N=20,30,40$ and 100. For OBC the finite-size effects are now pronounced for any $k_B T/K < 1$. It is natural to view this observation as being due to a considerable spatial size of the excitations responsible for the energy fluctuations. Most strikingly, for temperatures below $k_B T/K \sim 0.02 - 0.03$ a 'foot' of the specific heat can be observed with C_v almost constant over a considerable range of temperatures, albeit at a very low value. The value of C_v over this plateau appears to be decreasing with N . Unfortunately, due to size and temperature limitations it has not been possible to perform calculations at larger N , lower T . Since this 'foot' in C_v is only present for OBC at temperatures lower than for PBC it is clear that it most arise from excitations only present with OBC. We therefore ascribe this feature to the single soliton ground-state for OBC, excitations of which (Fig. 11) should significantly contribute to C_v at energies below Δ_{pbc} .

VIII. DISCUSSION

Here we discuss a few open questions and future directions. The variational picture of the soliton phase that we have been advocating here rely on the presence of a gap for periodic boundary conditions within the soliton phase. At the special point h_{xy}^* , the $|YX\rangle$ and $|XY\rangle$ product states are exact ground-states. It therefore seems plausible that an analytic proof of a gap at h_{xy}^* can be established. So far we have not been able to develop such a proof due to the low symmetry at h_{xy}^* and the degeneracy of the ground-state with PBC in the soliton phase.

Under open boundary conditions we have shown here that the ground-state for any N always contain a single soliton which can exist in excited states leading to the formation of in-gap states. Excited states of quantum solitons have been considered before [51, 70] and are usually associated with a discrete harmonic oscillator like spectrum. In the present case it is not clear if the in-gap states created by excitations of the soliton form a continuous band or if they form discrete states

in the thermodynamic limit. The energy of the lowest excited states appear to approach the ground-state quickly as N is increased but due to limitations in the size of the systems we can reliably study it has not been possible to determine if they indeed become degenerate with the ground-state in the thermodynamic limit. The degeneracy of the ground-state with OBC is hence an open question. We leave both these questions for further study.

As illustrated in Fig. 1 the size of the soliton islands grow with increasing S and one might ask the question what happens in the $S \rightarrow \infty$ classical limit. Classical Monte Carlo simulations are inconclusive in the low field limit but one might speculate that the soliton phase would occupy the entire phase diagram for any $|h| < 2S$ but so far we have not been able to establish a proof of this.

It would be of considerable interest to identify realistic low-dimensional Kitaev materials to test the soliton physics presented here. Recently it was proposed that CoNb_2O_6 exhibits signatures of Kitaev physics known as twisted Kitaev chain [105], albeit with $S=\frac{1}{2}$ FM Kitaev interaction and hence not the AFM Kitaev interaction required for our scenario. However, it seems likely that the AFM Kitaev interaction required for the soliton phase can occur in $S=1$ systems. Note that the effective $S=\frac{1}{2}$ Kitaev materials with d^5 have a predominantly FM Kitaev interaction as the inter-orbital exchange process among t_{2g} -orbitals leads to a FM Kitaev interaction[2, 106]. On the other hand, in $S=1$ systems with d^8 , the Kitaev interaction is AFM as found from the exchange processes of e_g -orbitals via strong spin-orbit coupling at anions [30]. It was also suggested that $4f^1$ system contains AFM Kitaev interaction due to the spatial anisotropy of the f orbitals and the small crystal field splitting.[107] Thus, the soliton phase occurring in the AFM Kitaev interaction under the magnetic field can be investigated if solid-state materials with quasi-one-dimensional d^8 systems and edge sharing heavy ligands or $4f^1$ can be identified. Since the solitons we have discussed here are particularly well defined for large integer spin, if such low-dimensional AFM Kitaev materials with large S can be found, it would offer the best possibility for observing the solitons. Finally, we remark that it would interesting to study the dynamics of the solitons in a non-equilibrium setting.

ACKNOWLEDGMENTS

This research was supported by NSERC and CIFAR and was enabled in part by support provided by SHARCNET (sharcnet.ca) and the Digital Research Alliance of Canada (alliancecan.ca). Part of the numerical calculations were per-

formed using the ITensor library [108].

Appendix A: The Generalized Eigenvalue Problem

Let us consider a set of states $\{|b_i\rangle\}_{i=1}^N$ and a Hamiltonian \mathcal{H} . We can expand a generic state $|\psi\rangle$ on such basis states writing

$$|\psi\rangle = \sum_{i=1}^N c_i |b_i\rangle \quad (\text{A1})$$

According to the variational principle the minimum condition is then written as the generalized eigenvalue problem

$$\sum_j (\mathcal{H}_{ij} - E\mathcal{M}_{ij}) c_j = 0, \quad (\text{A2})$$

where $\mathcal{H}_{ij} = \langle b_i | \mathcal{H} | b_j \rangle$ and \mathcal{M}_{ij} is the overlap matrix $\langle b_i | b_j \rangle$. In the case where $\langle b_i | b_j \rangle = \delta_{ij}$ this reduces to the standard eigenvalue problem. We can write Eq. (A2) in matrix form as

$$\mathcal{H}\mathbf{c} = E\mathcal{M}\mathbf{c}, \quad (\text{A3})$$

which defines a generalized eigenvalue problem. To solve Eq. (A3) we first solve the standard eigenvalue problem

$$\mathcal{M}\mathbf{d} = m\mathbf{d}. \quad (\text{A4})$$

If the states $\{|b_i\rangle\}_{i=1}^N$ are linearly independent then \mathcal{M} is positive definite and hermitian which implies we can find a unitary matrix D such that $D^\dagger \mathcal{M} D$ is a diagonal matrix. Since all $m > 0$ we can then define

$$A_{ij} \equiv \frac{D_{ij}}{\sqrt{m_j}} \quad (\text{A5})$$

so that $A^\dagger \mathcal{M} A = I$. If we now define

$$\mathbf{c} = A\mathbf{v}, \quad (\text{A6})$$

then Eq. (A3) can be written as

$$\mathcal{H}A\mathbf{v} = E\mathcal{M}A\mathbf{v}. \quad (\text{A7})$$

If we now apply the matrix A^\dagger from the left we then obtain

$$A^\dagger \mathcal{H} A \mathbf{v} = E A^\dagger \mathcal{M} A \mathbf{v} = E \mathbf{v}, \quad (\text{A8})$$

which is now a standard eigenvalue problem for the matrix $A^\dagger \mathcal{H} A$. We have then reduced the solution of the generalized eigenvalue problem to the solution of two standard eigenvalue problems.

[1] A. Y. Kitaev, Anyons in an exactly solved model and beyond, *Annals of Physics* **321**, 2 (2006).

[2] G. Jackeli and G. Khaliullin, Mott insulators in the strong spin-orbit coupling limit: From Heisenberg to a quantum compass

- and Kitaev models, *Phys. Rev. Lett.* **102**, 017205 (2009).
- [3] W. Witczak-Krempa, G. Chen, Y. B. Kim, and L. Balents, Correlated quantum phenomena in the strong spin-orbit regime, *Annual Review of Condensed Matter Physics* **5**, 57 (2014).
- [4] J. G. Rau, E. K.-H. Lee, and H.-Y. Kee, Spin-orbit physics giving rise to novel phases in correlated systems: Iridates and related materials, *Annual Review of Condensed Matter Physics* **7**, 195 (2016).
- [5] S. M. Winter, A. A. Tsirlin, M. Daghofer, J. van den Brink, Y. Singh, P. Gegenwart, and R. Valentí, Models and materials for generalized Kitaev magnetism, *Journal of Physics: Condensed Matter* **29**, 493002 (2017).
- [6] M. Hermanns, I. Kimchi, and J. Knolle, Physics of the Kitaev model: Fractionalization, dynamic correlations, and material connections, *Annual Review of Condensed Matter Physics* **9**, 17 (2018).
- [7] L. Janssen and M. Vojta, Heisenberg-kitaev physics in magnetic fields, *Journal of Physics: Condensed Matter* **31**, 423002 (2019).
- [8] H. Takagi, T. Takayama, G. Jackeli, G. Khaliullin, and S. E. Nagler, Concept and realization of kitaev quantum spin liquids, *Nature Reviews Physics* **1**, 264 (2019).
- [9] S. Trebst and C. Hickey, Kitaev materials, *Physics Reports* **950**, 1 (2022).
- [10] Y. Kasahara, T. Ohnishi, Y. Mizukami, O. Tanaka, S. Ma, K. Sugii, N. Kurita, H. Tanaka, J. Nasu, Y. Motome, T. Shibauchi, and Y. Matsuda, Majorana quantization and half-integer thermal quantum hall effect in a kitaev spin liquid, *Nature* **559**, 227 (2018).
- [11] T. Yokoi, S. Ma, Y. Kasahara, S. Kasahara, T. Shibauchi, N. Kurita, H. Tanaka, J. Nasu, Y. Motome, C. Hickey, S. Trebst, and Y. Matsuda, Half-integer quantized anomalous thermal hall effect in the kitaev material candidate α -rucl₃, *Science* **373**, 568 (2021).
- [12] P. Czajka, T. Gao, M. Hirschberger, P. Lampen-Kelley, A. Banerjee, J. Yan, D. G. Mandrus, S. E. Nagler, and N. P. Ong, Oscillations of the thermal conductivity in the spin-liquid state of α -rucl₃, *Nature Physics* **17**, 915 (2021).
- [13] J. A. N. Bruin, R. R. Claus, Y. Matsumoto, N. Kurita, H. Tanaka, and H. Takagi, Robustness of the thermal hall effect close to half-quantization in α -rucl₃, *Nature Physics* **18**, 401 (2022).
- [14] P. Czajka, T. Gao, M. Hirschberger, P. Lampen-Kelley, A. Banerjee, N. Quirk, D. G. Mandrus, S. E. Nagler, and N. P. Ong, Planar thermal hall effect of topological bosons in the kitaev magnet α -rucl₃, *Nature Materials* [10.1038/s41563-022-01397-w](https://doi.org/10.1038/s41563-022-01397-w) (2022).
- [15] X.-G. Zhou, H. Li, Y. H. Matsuda, A. Matsuo, W. Li, N. Kurita, K. Kindo, and H. Tanaka, Intermediate quantum spin liquid phase in the kitaev material α -rucl₃ under high magnetic fields up to 100 t (2022), [arXiv:2201.04597](https://arxiv.org/abs/2201.04597).
- [16] Z. Zhu, I. Kimchi, D. N. Sheng, and L. Fu, Robust non-abelian spin liquid and a possible intermediate phase in the antiferromagnetic kitaev model with magnetic field, *Phys. Rev. B* **97**, 241110(R) (2018).
- [17] J. Nasu, Y. Kato, Y. Kamiya, and Y. Motome, Successive majorana topological transitions driven by a magnetic field in the kitaev model, *Phys. Rev. B* **98**, 060416(R) (2018).
- [18] S. Liang, M.-H. Jiang, W. Chen, J.-X. Li, and Q.-H. Wang, Intermediate gapless phase and topological phase transition of the kitaev model in a uniform magnetic field, *Phys. Rev. B* **98**, 054433 (2018).
- [19] M. Gohlke, R. Moessner, and F. Pollmann, Dynamical and topological properties of the kitaev model in a [111] magnetic field, *Phys. Rev. B* **98**, 014418 (2018).
- [20] H.-C. Jiang, C.-Y. Wang, B. Huang, and Y.-M. Lu, Field induced quantum spin liquid with spinon fermi surfaces in the Kitaev model (2018), [arXiv:1809.08247](https://arxiv.org/abs/1809.08247).
- [21] C. Hickey and S. Trebst, Emergence of a field-driven u(1) spin liquid in the kitaev honeycomb model, *Nature Communications* **10**, 530 (2019).
- [22] N. D. Patel and N. Trivedi, Magnetic field-induced intermediate quantum spin liquid with a spinon fermi surface, *Proceedings of the National Academy of Sciences* **116**, 12199 (2019).
- [23] L. Zou and Y.-C. He, Field-induced qcd₃-chern-simons quantum criticalities in kitaev materials, *Phys. Rev. Research* **2**, 013072 (2020).
- [24] J. S. Gordon, A. Catuneanu, E. S. Sørensen, and H.-Y. Kee, Theory of the field-revealed kitaev spin liquid, *Nature Communications* **10**, 2470 (2019).
- [25] D. A. S. Kaib, S. M. Winter, and R. Valentí, Kitaev honeycomb models in magnetic fields: Dynamical response and dual models, *Phys. Rev. B* **100**, 144445 (2019).
- [26] H.-Y. Lee, R. Kaneko, L. E. Chern, T. Okubo, Y. Yamaji, N. Kawashima, and Y. B. Kim, Magnetic field induced quantum phases in a tensor network study of kitaev magnets, *Nature Communications* **11**, 1639 (2020).
- [27] H. Li, H.-K. Zhang, J. Wang, H.-Q. Wu, Y. Gao, D.-W. Qu, Z.-X. Liu, S.-S. Gong, and W. Li, Identification of magnetic interactions and high-field quantum spin liquid in α -rucl₃, *Nature Communications* **12**, 4007 (2021).
- [28] G. Baskaran, D. Sen, and R. Shankar, Spin- s kitaev model: Classical ground states, order from disorder, and exact correlation functions, *Phys. Rev. B* **78**, 115116 (2008).
- [29] I. Rousochatzakis, Y. Szyuk, and N. B. Perkins, Quantum spin liquid in the semiclassical regime, *Nature Communications* **9**, 1575 (2018).
- [30] P. P. Stavropoulos, D. Pereira, and H.-Y. Kee, Microscopic mechanism for a higher-spin kitaev model, *Phys. Rev. Lett.* **123**, 037203 (2019).
- [31] A. Koga, T. Minakawa, Y. Murakami, and J. Nasu, Spin transport in the quantum spin liquid state in the $s = 1$ kitaev model: Role of the fractionalized quasiparticles, *Journal of the Physical Society of Japan* **89**, 033701 (2020).
- [32] X.-Y. Dong and D. N. Sheng, Spin-1 kitaev-heisenberg model on a honeycomb lattice, *Phys. Rev. B* **102**, 121102(R) (2020).
- [33] Z. Zhu, Z.-Y. Weng, and D. N. Sheng, Magnetic field induced spin liquids in $s = 1$ kitaev honeycomb model, *Phys. Rev. Research* **2**, 022047(R) (2020).
- [34] I. Khait, P. P. Stavropoulos, H.-Y. Kee, and Y. B. Kim, Characterizing spin-one kitaev quantum spin liquids, *Phys. Rev. Research* **3**, 013160 (2021).
- [35] Y.-H. Chen, J. Genzor, Y. B. Kim, and Y.-J. Kao, Excitation spectrum of spin-1 kitaev spin liquids, *Phys. Rev. B* **105**, L060403 (2022).
- [36] C. Hickey, C. Berke, P. P. Stavropoulos, H.-Y. Kee, and S. Trebst, Field-driven gapless spin liquid in the spin-1 kitaev honeycomb model, *Phys. Rev. Research* **2**, 023361 (2020).
- [37] E. S. Sørensen, J. Gordon, J. Riddell, and H.-Y. Kee, Field induced chiral soliton phase in the kitaev spin chain (2022), [arXiv:2209.06221](https://arxiv.org/abs/2209.06221).
- [38] E. S. Sørensen, A. Catuneanu, J. S. Gordon, and H.-Y. Kee, Heart of entanglement: Chiral, nematic, and incommensurate phases in the kitaev-gamma ladder in a field, *Phys. Rev. X* **11**, 011013 (2021).
- [39] D. Sen, R. Shankar, D. Dhar, and K. Ramola, Spin-1 kitaev model in one dimension, *Phys. Rev. B* **82**, 195435 (2010).

- [40] Q. Luo, S. Hu, and H.-Y. Kee, Unusual excitations and double-peak specific heat in a bond-alternating spin-1 $k - \Gamma$ chain, *Phys. Rev. Research* **3**, 033048 (2021).
- [41] G.-H. Liu, L.-J. Kong, and W.-L. You, Quantum phase transitions in spin-1 compass chains, *The European Physical Journal B* **88**, 284 (2015).
- [42] W.-L. You, G. Sun, J. Ren, W. C. Yu, and A. M. Oleś, Quantum phase transitions in the spin-1 kitaev-heisenberg chain, *Phys. Rev. B* **102**, 144437 (2020).
- [43] W.-L. You, Z. Zhao, J. Ren, G. Sun, L. Li, and A. M. Olés, Quantum many-body scars in spin-1 kitaev chains, *Phys. Rev. Res.* **4**, 013103 (2022).
- [44] K.-W. Sun and Q.-H. Chen, Quantum phase transition of the one-dimensional transverse-field compass model, *Physical Review B* **80**, 174417 (2009).
- [45] H. J. Mikeska, Solitons in a one-dimensional magnet with an easy plane, *Journal of Physics C: Solid State Physics* **11**, L29 (1978).
- [46] H. J. Mikeska, Non-linear dynamics of classical one-dimensional antiferromagnets, *Journal of Physics C: Solid State Physics* **13**, 2913 (2000).
- [47] H. C. Fogedby, Solitons and magnons in the classical Heisenberg chain, *Journal of Physics A: Mathematical and General* **13**, 1467 (1980).
- [48] H. C. Fogedby, The spectrum of the continuous isotropic quantum Heisenberg chain: quantum solitons as magnon bound states, *Journal of Physics C: Solid State Physics* **13**, L195 (1980).
- [49] H.-J. Mikeska and M. Steiner, Solitary excitations in one-dimensional magnets, *Advances in Physics* **40**, 191 (1991).
- [50] A. Kosevich, B. Ivanov, and A. Kovalev, Magnetic Solitons, *Physics Reports* **194**, 117 (1990).
- [51] T. Vachaspati, *Kinks and Domain Walls* (Cambridge University Press, 2006).
- [52] T. Dauxois and M. Peyrard, *Physics of Solitons* (Cambridge University Press, 2006).
- [53] A. J. Heeger, S. Kivelson, J. R. Schrieffer, and W. P. Su, Solitons in conducting polymers, *Reviews of Modern Physics* **60**, 781 (1988).
- [54] J. K. Kjems and M. Steiner, Evidence for Soliton Modes in the One-Dimensional Ferromagnet CsNiF₃, *Physical Review Letters* **41**, 1137 (1978).
- [55] J. P. Boucher, F. Mezei, L. P. Regnault, and J. P. Renard, Diffusion of solitons in the antiferromagnetic chains of (CD₃)₄NMnCl₃: A study by neutron spin echo, *Physical Review Letters* **55**, 1778 (1985).
- [56] L. P. Regnault, J. P. Boucher, J. Rossat-Mignod, J. P. Renard, J. Bouillot, and W. G. Stirling, A neutron investigation of the soliton regime in the one-dimensional planar antiferromagnet (cd₃)₄nmncl₃, *Journal of Physics C: Solid State Physics* **15**, 1261 (1982).
- [57] W. J. L. Buyers, M. J. Hogan, R. L. Armstrong, and B. Briat, Solitons in the one-dimensional ising-like antiferromagnet CsCoBr₃, *Phys. Rev. B* **33**, 1727 (1986).
- [58] H.-B. Braun, J. Kulda, B. Roessli, D. Visser, K. W. Krämer, H.-U. Güdel, and P. Böni, Emergence of soliton chirality in a quantum antiferromagnet, *Nature Physics* **1**, 159 (2005).
- [59] B. D. Gaulin and M. F. Collins, Evidence for out-of-easy-plane solitons in CsMnBr₃, *Canadian Journal of Physics* **63**, 1235 (1985), <https://doi.org/10.1139/p85-202>.
- [60] B. D. Gaulin, M. F. Collins, and W. J. L. Buyers, Spin waves in the triangular antiferromagnet csmnbr₃, *Journal of Applied Physics* **61**, 3409 (1987).
- [61] B. D. Gaulin, Soliton spin configurations along the classical anisotropic heisenberg chain, *Journal of Applied Physics* **61**, 4435 (1987).
- [62] B. S. Shastry and B. Sutherland, Excitation spectrum of a dimerized next-neighbor antiferromagnetic chain, *Phys. Rev. Lett.* **47**, 964 (1981).
- [63] W. J. Caspers and W. Magnus, Some exact excited states in a linear antiferromagnetic spin system, *Phys. Lett. A* **88A**, 103 (1982).
- [64] W. J. Caspers, K. M. Emmett, and W. Magnus, The majumdar-gosh chain. twofold ground state and elementary excitations, *J. Phys. A* **17**, 2687 (1984).
- [65] E. Sørensen, I. Affleck, D. Augier, and D. Poilblanc, Soliton approach to spin-peierls antiferromagnets: Large-scale numerical results, *Phys. Rev. B* **58**, R14701 (1998).
- [66] E. S. Sørensen, M.-S. Chang, N. Laflorencie, and I. Affleck, Impurity entanglement entropy and the kondo screening cloud, *Journal of Statistical Mechanics: Theory and Experiment* **2007**, L01001 (2007).
- [67] E. S. Sørensen, M.-S. Chang, N. Laflorencie, and I. Affleck, Quantum impurity entanglement, *Journal of Statistical Mechanics: Theory and Experiment* **2007**, P08003 (2007).
- [68] F. Casola, T. Shiroka, A. Feiguin, S. Wang, M. S. Grbić, M. Horvatić, S. Krämer, S. Mukhopadhyay, K. Conder, C. Berthier, H.-R. Ott, H. M. Rønnow, C. Rüegg, and J. Mesot, Field-induced quantum soliton lattice in a frustrated two-leg spin-1/2 ladder, *Phys. Rev. Lett.* **110**, 187201 (2013).
- [69] M. Horvatić, Y. Fagot-Revurat, C. Berthier, G. Dhalle, and A. Revcolevschi, Nmr imaging of the soliton lattice profile in the spin-peierls compound cugeo₃, *Phys. Rev. Lett.* **83**, 420 (1999).
- [70] R. Rajaraman, *Solitons and Instatons* (North-Holland, 1987).
- [71] J. S. Gordon and H.-Y. Kee, Insights into the anisotropic spin-s kitaev chain, *Phys. Rev. Research* **4**, 013205 (2022).
- [72] N. Schuch, D. Pérez-García, and I. Cirac, Classifying quantum phases using matrix product states and projected entangled pair states, *Phys. Rev. B* **84**, 165139 (2011).
- [73] X. Chen, Z.-C. Gu, and X.-G. Wen, Classification of gapped symmetric phases in one-dimensional spin systems, *Phys. Rev. B* **83**, 035107 (2011).
- [74] X.-G. Wen, Colloquium: Zoo of quantum-topological phases of matter, *Rev. Mod. Phys.* **89**, 041004 (2017).
- [75] F. Pollmann and A. M. Turner, Detection of symmetry-protected topological phases in one dimension, *Phys. Rev. B* **86**, 125441 (2012).
- [76] F. Pollmann, A. M. Turner, E. Berg, and M. Oshikawa, Entanglement spectrum of a topological phase in one dimension, *Phys. Rev. B* **81**, 064439 (2010).
- [77] F. Pollmann, E. Berg, A. M. Turner, and M. Oshikawa, Symmetry protection of topological phases in one-dimensional quantum spin systems, *Phys. Rev. B* **85**, 075125 (2012).
- [78] Y. Fuji, F. Pollmann, and M. Oshikawa, Distinct trivial phases protected by a point-group symmetry in quantum spin chains, *Phys. Rev. Lett.* **114**, 177204 (2015).
- [79] A. Kshetrimayum, H.-H. Tu, and R. Orús, Symmetry-protected intermediate trivial phases in quantum spin chains, *Phys. Rev. B* **93**, 245112 (2016).
- [80] L. Tsui, H.-C. Jiang, Y.-M. Lu, and D.-H. Lee, Quantum phase transitions between a class of symmetry protected topological states, *Nuclear Physics B* **896**, 330 (2015).
- [81] F. Verstraete, J. J. García-Ripoll, and J. I. Cirac, Matrix product density operators: Simulation of finite-temperature and dissipative systems, *Phys. Rev. Lett.* **93**, 207204 (2004).

- [82] X. Chen, Z.-C. Gu, Z.-X. Liu, and X.-G. Wen, Symmetry protected topological orders and the group cohomology of their symmetry group, *Phys. Rev. B* **87**, 155114 (2013).
- [83] S. R. White and R. M. Noack, Real-space quantum renormalization groups, *Phys. Rev. Lett.* **68**, 3487 (1992).
- [84] S. R. White, Density matrix formulation for quantum renormalization groups, *Phys. Rev. Lett.* **69**, 2863 (1992).
- [85] S. R. White, Density-matrix algorithms for quantum renormalization groups, *Phys. Rev. B* **48**, 10345 (1993).
- [86] U. Schollwöck, The density-matrix renormalization group, *Rev. Mod. Phys.* **77**, 259 (2005).
- [87] K. A. Hallberg, New trends in density matrix renormalization, *Advances in Physics* **55**, 477 (2006).
- [88] U. Schollwöck, The density-matrix renormalization group in the age of matrix product states, *Annals of Physics* **326**, 96 (2011), january 2011 Special Issue.
- [89] I. P. McCulloch, Infinite size density matrix renormalization group, revisited, ArXiv.org [arXiv:0804.2509](https://arxiv.org/abs/0804.2509) (2008).
- [90] A. F. Albuquerque, F. Alet, C. Sire, and S. Capponi, Quantum critical scaling of fidelity susceptibility, *Physical Review B* **81**, 064418 (2010).
- [91] A. Uhlmann, The “transition probability” in the state space of a $*$ -algebra, *Reports on Mathematical Physics* **9**, 273 (1976).
- [92] A. Uhlmann, Parallel transport and “quantum holonomy” along density operators, *Reports on Mathematical Physics* **24**, 229 (1986).
- [93] T. Barthel, U. Schollwöck, and S. R. White, Spectral functions in one-dimensional quantum systems at finite temperature using the density matrix renormalization group, *Phys. Rev. B* **79**, 245101 (2009).
- [94] C. Karrasch, J. H. Bardarson, and J. E. Moore, Finite-temperature dynamical density matrix renormalization group and the drude weight of spin-1/2 chains, *Phys. Rev. Lett.* **108**, 227206 (2012).
- [95] T. Barthel, One-dimensional quantum systems at finite temperatures can be simulated efficiently on classical computers (2017), [arXiv:1708.09349](https://arxiv.org/abs/1708.09349).
- [96] J. Hauschild, E. Leviatan, J. H. Bardarson, E. Altman, M. P. Zaletel, and F. Pollmann, Finding purifications with minimal entanglement, *Phys. Rev. B* **98**, 235163 (2018).
- [97] W. Israel, hermo field dynamics, *Collect. Phenom.* **2**, 55 (1975).
- [98] W. Israel, Thermo-field dynamics of black holes, *Physics Lett. A* **57**, 107 (1976).
- [99] J. Goldstone and R. Jackiw, Quantization of nonlinear waves, *Phys. Rev. D* **11**, 1486 (1975).
- [100] R. J. Bursill, T. Xiang, and G. A. Gehring, The density matrix renormalization group for a quantum spin chain at non-zero temperature, *Journal of Physics: Condensed Matter* **8**, L583 (1996).
- [101] X. Wang and T. Xiang, Transfer-matrix density-matrix renormalization-group theory for thermodynamics of one-dimensional quantum systems, *Phys. Rev. B* **56**, 5061 (1997).
- [102] J. Nasu, M. Udagawa, and Y. Motome, Thermal fractionalization of quantum spins in a kitaev model: Temperature-linear specific heat and coherent transport of majorana fermions, *Phys. Rev. B* **92**, 115122 (2015).
- [103] Y. Motome and J. Nasu, Hunting majorana fermions in kitaev magnets, *Journal of the Physical Society of Japan* **89**, 012002 (2020).
- [104] J. Oitmaa, A. Koga, and R. R. P. Singh, Incipient and well-developed entropy plateaus in spin- s kitaev models, *Phys. Rev. B* **98**, 214404 (2018).
- [105] C. M. Morris, N. Desai, J. Viirok, D. Huvonen, U. Nagel, T. Room, J. W. Krizan, R. J. Cava, T. M. McQueen, S. M. Koohpayeh, R. K. Kaul, and N. P. Armitage, Duality and domain wall dynamics in a twisted kitaev chain, *Nature Physics* **17**, 832 (2021).
- [106] J. G. Rau, E. K.-H. Lee, and H.-Y. Kee, Generic spin model for the honeycomb iridates beyond the kitaev limit, *Phys. Rev. Lett.* **112**, 077204 (2014).
- [107] Y. Motome, R. Sano, S. Jang, Y. Sugita, and Y. Kato, Materials design of kitaev spin liquids beyond the jackeli–khaliullin mechanism, *Journal of Physics: Condensed Matter* **32**, 404001 (2020).
- [108] M. Fishman, S. R. White, and E. M. Stoudenmire, The ITensor software library for tensor network calculations (2020), [arXiv:2007.14822](https://arxiv.org/abs/2007.14822).